Nanoscale

Accepted Manuscript

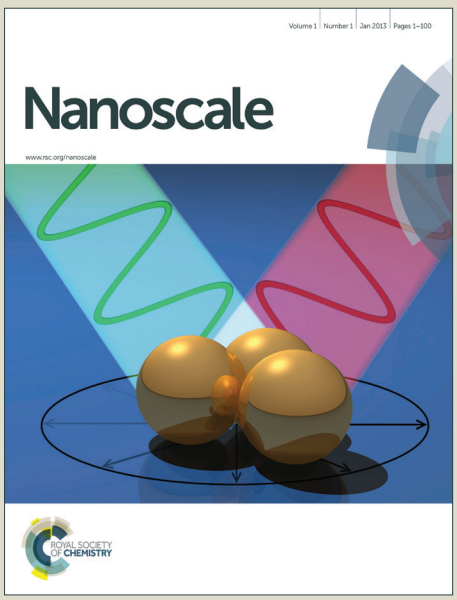

ROYAL SOCIETY OF CHEMISTRY

www.rsc.org/nanoscale

Journal Name

RSCPublishing

ARTICLE

A comprehensive review of the application of chalcogenide nanoparticles in polymer solar cells

Cite this: DOI: 10.1039/x0xx00000x

J. N. Freitas,[a,b,*] A. S. Gonçalves[b] and A. F. Nogueira[b,*]

Received 00th January 2012,
Accepted 00th January 2012

DOI: 10.1039/x0xx00000x

www.rsc.org/

In this review the use of solution-processed chalcogenide quantum dots (CdS, CdSe, PbS, etc.) in hybrid organic-inorganic solar cells is explored. Such devices are known as potential candidates for low-cost and efficient solar energy conversion, and compose the so called Third Generation Solar Cells. The incorporation of oxides and metal nanoparticles has also been successfully attained in this new class of photovoltaic devices; however, we choose to explore here the chalcogenide quantum dots in light of their particularly attractive optical and electronic properties. We address herein a comprehensive review of the historical background and state-of-the-art comprising the incorporation of such nanoparticles in polymer matrixes. Later strategies for surface chemistry manipulation, *in-situ* synthesis of nanoparticles, use of continuous 3D nanoparticles network (aerogels) and ternary systems are also reviewed.

Polymer/quantum dot hybrid organic-inorganic solar cells

Inorganic nanoparticles with quantum confinement properties, quantum dots (QDs), have been largely used in optoelectronic devices. Their properties such as absorption, emission, electron affinity, etc, depend on the size (diameter) of the nanoparticle. For example, as the nanoparticle diameter decreases, the absorption maximum is blue-shifted, as a result of a change in the band gap energy due to the quantum confinement effect. Figure 1 illustrates the changes in luminescence emission of CdSe(ZnS) QDs when the size increases from 2 to 6 nm. In addition to the quantum confinement effect, inorganic nanoparticles have the advantage that they can be easily synthesized in a great variety of shapes, such as spheres, prisms, rods, wires, and even larger and more complex structures, such as tetrapods or hyperbranched nanocrystals (Figure 2). The fundamental properties and synthesis strategies involving QDs will not be discussed here, and can be found in excellent reviews published elsewhere [1,2,3,4].

Insert Fig 1 here

Figure 1. Luminescence emission from CdSe(ZnS) quantum dots solutions: the size of the nanoparticles increases from ~ 2 nm to ~ 6 nm (left to the right). The emission spans across the visible part of the electromagnetic spectrum from the blue (2 nm nanocrystals) to the red (6 nm nanocrystals). Reprinted with permission from reference [5]. Copyright 2009, Elsevier.

Considering their application in photovoltaic devices, QDs have to be combined with a second material, which can be a hole transporter, such as conjugated polymers, an electron transporter material, such as metal oxides or fullerenes, or a metal electrode.

Insert Fig 2 here

Figure 2. Structural depictions and approximate dimensions of nanomaterials used in polymer and hybrid organic-inorganic photovoltaic cells, such as chalcogenide nanoparticles. The size ranges shown are estimates based on literature reports for these materials and carbon-based nanomaterials usually employed in "classical" organic solar cells (PCBM, $PC_{71}BM$ and SWNT). Reprinted with permission from reference [6]. Copyright 2008, Elsevier.

Hybrid organic-inorganic polymer/QD mixtures offer appealing possibilities to explore the best of both components: the solution processing ability of the semiconducting polymers and the high electron mobility and transport properties of inorganic semiconductors. In these devices, the conducting polymer acts as the hole transport material, and the inorganic component as the electron acceptor and electron transport material.

Hybrid polymer/QD devices offer a series of advantages over more traditional polymer/fullerene systems. Some of the expected advantages are: (i) the contribution to light absorption by an inorganic acceptor can also lead to the photogeneration of charge carriers, which could be greater than the absorption contribution of fullerene derivatives; (ii) the absorption of QDs can be tuned to cover a broad spectral range, as a result of modification of size and shape of inorganic nanoparticles, thus offering the possibility of choosing the spectral window for complementary absorption profile in relation to the polymer; (iii) the physical dimensions of some inorganic semiconductors can be tailored via some synthesis methods to produce 1D nanostructures, which are expected to allow efficient excitonic

dissociation and electron transporting pathways simultaneously; and inorganic QDs are expected to (iv) provide ultrafast photoinduced charge carrier transfer to organic semiconductors, leading to efficient charge transfer between donor and acceptor materials; (v) have relatively high electron mobility and (vi) have good photo- and chemical stability.

On the other hand, in hybrid organic-inorganic devices, an improved molecular level control of the system and a deeper scientific understanding of structure/processing/property relationships are still necessary. Device efficiencies currently achieved for hybrid solar cells are significantly lower than polymer/fullerene devices. This is mainly related to the fact that achieving a controllable continuous percolation network, and a well-defined interface between QDs and the polymer matrix, remains challenging. Phase separation of inorganic nanoparticles from conjugated polymers might decrease interfacial area. Furthermore, the presence of surface traps in the QDs might affect charge generation and charge transport.

While extensive literature and reviews have been published in the last couple years about polymer/QD solar cells, usually the reports provide a summary of the essential and most useful results, and champion devices. In this review, our goal is to provide a more comprehensive view of the background and the state-of-the-art of polymer/QD solar cells, wherein the reader has the opportunity to go through all kinds of results, i.e., from low efficiency devices to the record ones. We believe this analysis can be particularly useful for young research groups starting in this area to gather experience, and to illustrate the heterogeneity of results that can be achieved when working with these systems. We also revise approaches based on surface chemistry manipulation, *in-situ* nanoparticles synthesis and use of continuous 3D nanoparticles network (aerogels), which could inspire a next generation of hybrid devices. Last, but not least, a section dedicated to ternary systems, in which QDs are incorporated as additives to polymer/fullerene devices, is included. Ternary systems based on combinations of three materials, not necessarily involving inorganic materials, have recently come to focus. The fact that they are now considered a suitable strategy is reflected in several reviews about ternary-based solar cells published lately [7,8,9]. Most reviews give a broad panorama on ternary systems, comprising an analysis of all kinds of ternary mixtures, without giving particular attention and comprehensive literature on polymer/fullerene/QD systems. Here we will focus in ternary devices containing chalcogenide QDs and on providing a comprehensive view of the evolution in this field.

The fundamental properties and device operation principles of polymer/QD solar cells will not be revised here, but can be found in recent reviews published elsewhere [10,11,12,13,14,15,16,17].

The use of nonchalcogenide nanoparticles in solar cells, or the use of QDs as sensitizers for oxide films (QDDSSCs) will not be addressed in this review as well. These are exciting topics and readers are directed to excellent reviews about the application of nonchalcogenide nanoparticles in solar cells[12,15,18,19] and QDDSSCs[13,20,21,22,23] published elsewhere.

Cd-based chalcogenides

In 1996, inspired by organic solar cells based on polymer/fullerene mixtures, Greenham et al. [24] studied the photoluminescence and photoconductivity of the materials formed with mixtures of poly(1-methoxy-4-(2-ethylhexyloxy-2,5-phenylenevinylene)) (MEH-PPV) and either CdS or CdSe nanoparticles. The authors showed that efficient photoconductivity could be achieved at high nanocrystal concentrations, when electrons and holes could be transported, respectively, through the inorganic and polymer components of the composite material. This was a breakthrough work. Nevertheless, it was only after the classical report by Huynh et al. [25] in 2002 that bulk heterojunction polymer/QD mixtures based on chalcogenide nanoparticles became really popular for application in solar cells. To date, this work is considered a case of success and continues to be one of the most cited reports in polymer/QD literature. The authors combined CdSe spherical nanoparticles (7 nm diameter) or CdSe nanorods (7 nm x 60 nm dimensions) with poly(3-hexylthiophene) (P3HT) and observed that the maximum external quantum efficiency (EQE) value increased from ~ 20 % to ~ 55 % when nanospheres were substituted by nanorods (Figure 3). The best device delivered a short-circuit current (Jsc) of 5.7 mA cm^{-2}, and open-circuit voltage (Voc) of 0.7 V and fill factor (FF) of 40 %, with a power conversion efficiency (PCE) of 1.7 %. As the aspect ratio of the nanorods increased from 1 to 10, the charge transport improved. It is expected that, in networks consisting of shorter nanoparticles, electron transport is dominated by hopping and, while in those consisting of longer particles, band conduction is prevalent [25].

Insert Fig 3 here

Figure 3. EQE of hybrid devices assembled with CdSe 7-nm-diameter nanorods with lengths 7, 30, and 60 nm, combined with P3HT. The intensity is 0.084 mW cm^{-2} at 515 nm. Reprinted with permission from [25]. Copyright 2002, The American Association for the Advancement of Science.

Hindson et al. [26] showed with electron tomography in high-angle annular dark-field scanning transmission electron microscopy that the use of nanorods instead of spherical particles results in a highly connected network of particles homogeneously distributed through the polymer film, as displayed in Figure 4. The nanorod/polymer films were found to be more spatially homogeneous than the spherical QD/polymer films.

Insert Fig 4 here

Figure 4. Images of the binarized tomographic data. The purple regions are the CdSe particles while the polymer regions are transparent. Low-density regions are shown for (a) 6:1, (b) 3:1, and (c) 2:1 nanodot-polymer blends by weight. (d) Typical aggregated region in a 6:1 nanodot-polymer blend. (e) Nanorod-polymer blend. Reprinted with permission from [26]. Copyright 2002, American Chemical Society.

Other structures, such as tetrapods [27,28] and hyperbranched nanocrystals [29] based on CdSe, CdTe and $CdSe_xTe_{1-x}$ have also been used in combination with P3HT or poly[2-methoxy-5-

(3,7-dimethyloctyloxy)]-1,4-phenylenevinylene (MDMO-PPV), resulting in devices with efficiencies around 1-2 %. A comparison of the performance of solar cells assembled with CdSe nanorods or tetrapods performed by Sun et al. [28] in 2003 showed that the branched nanoparticles lead to more efficient devices, due to more extended electric pathways provided by the elongated and branched particles. It was also reported that charge separation occurs quickly if the exciton is generated in a CdSe branch which is in direct contact with the P3HT phase [30]. Besides, the use of longer armed tetrapods seems to aid in a better spatial connectivity. Such connectivity is desirable and contributes to decrease charge hopping events, leading to better charge transport [31]. Dayal et al. [32] have shown with microwave conductivity measurements that the increased aspect ratio from dots to rods to tetrapods particles provides conduits for electrons to move away from the dissociation sites, thus improving the generation of long-lived charge carriers.

In 2005, Sun et al. [33] combined CdSe tetrapods with P3HT and the films were spin-casted from 1,2,4-trichlorobenzene solutions. The devices delivered efficiencies of 2.4 %, much higher than the efficiencies of ~0.7 % obtained with films deposited from chloroform solutions. The impressive change in device performance based on different solvents indicated that the processing conditions induce different physical structures and could be a key to more efficient devices. In fact, it was quickly found that the manipulation of morphology during the deposition of hybrid films is a key parameter in these systems, and morphology is significantly affected by the solvent used during film deposition. In 2003, Huynh et al. [34] had demonstrated that the use of binary solvent mixtures could be used to control QDs dispersion in the polymer. By varying the concentration of the pyridine/chloroform solvent mixture, where pyridine is a ligand for the nanoparticles, phase separation was tuned from micrometer scale to nanometer scale. Other works also reported that by optimizing the solvent mixture used during film deposition, higher efficiencies could be achieved [35,36,37].

In 2010, a record efficiency of 3.13 % (Jsc ~ 9.0 mA cm^{-2}, Voc ~ 0.67 mV and FF ~ 51 %) was reported by Dayal et al. [38] for a bulk heterojunction solar cell assembled with CdSe tetrapods and the low band gap polymer PCPDTBT (poly[2,6-(4,4-bis-(2-ethylhexyl)-4H-cyclopenta[2,1-b;3,4-b′]dithiophene)-alt-4,7-(2,1,3-benzothiadiazole)). The success of this device was attributed to a combination of the tetrapods advantages with improved light-harvesting properties of PCPDTBT. Figure 5 shows the structure of PCPDTBT and P3HT, and the EQE spectra of the devices based on P3HT:CdSe and PCPDTBT:CdSe mixtures. The PCPDTBT-based device showed a broader EQE spectrum from 300 to 850 nm, in consistence with a broader absorption spectrum of this polymer compared to P3HT.

Insert Fig 5 here

Figure 5. (a) Schematic energy level diagram of P3HT, PCPDTBT, and CdSe QDs (spherical particles with a diameter of ~4.7 nm), and the chemical structure of the polymers. (b) EQE spectra of the P3HT:CdSe and the PCPDTBT:CdSe hybrid solar cells. In this particular case, CdSe nanoparticles are in the spherical form. Reprinted with permission from reference [44]. Copyright 2011, Elsevier.

In 2012, an even higher efficiency of 3.42 % was reported by Celik et al. [39]. Interestingly, this was achieved by using a combination of PCPDTBT, the same polymer used by Dayal et al. [38], but employing CdSe nanorods instead of the tetrapods. Celik et al. [39] performed a series of washing steps with methanol and n-hexane, followed by ligand exchange with pyridine, which led to the removal of excess free ligands that remain around the QD surface. The best device presented Jsc of 12.1 mA cm^{-2}, Voc of 0.63 mV, FF of 45 % and PCE of 3.42 % at the 27th day of measurement [39].

For a while it seemed that branched, complex chalcogenides structures were required to make successful polymer/chalcogenide devices. Many attempts to make devices using spherical nanoparticles resulted in efficiencies below 1 %. For example, in 2006, Han et al. [37] used spherical CdSe nanoparticles crystallized in zinc blend structure, with 4.5 nm of diameter, covered with 1-octadecene and oleic acid and combined with MEH-PPV in solar cells. After annealing, devices delivered an efficiency of 0.85 % (Jsc ~ 2.0 mA cm^{-2}, Voc ~0.90 V and FF ~ 47 %). Other reports combining CdSe spherical particles with P3HT or MEH-PPV showed efficiencies even lower, below 0.1 % [40,41]. Efficiency values of ~ 2 % for hybrid solar cells using a combination of spherical CdSe nanoparticles with P3HT were reported only in 2010, by Zhou et al. [42,43]. This was achieved by treating the nanoparticles with hexanoic acid, which removed the excess of surfactants accumulated around the QDs surfaces and, therefore, improved the charge transfer processes.

In 2011, Zhou et al. [44] applied the acid-assisted washing procedure to different ligand-capped CdSe QDs, which were then mixed with the low bandgap polymer PCPDTBT. The photovoltaic devices were optimized with respect to the polymer:CdSe ratio, photoactive film thickness, thermal annealing, and the use of different cathode materials, leading a record efficiency of 2.7 % for a spherical CdSe QD-based hybrid solar cell after spectral mismatch corrections (Jsc ~ 8.2 mA cm^{-2}, Voc ~0.59 V and FF ~ 55 %). The same group reported optimized devices using hexanoic-acid-treated CdSe QDs with a mean diameter of 7.1 ± 0.4 nm and PCPDTBT, exhibiting a further improvement of the PCE up to 3.1 % [45]. In this work, three strategies were used: (a) QDs with a reduced ligand shell (via acid treatment); (b) large-sized QDs, and (c) QD:nanorod mixtures. Initially, it was demonstrated that acid treated QDs exhibited higher efficiencies than non-treated ones, since the connectivity of the interpenetrating nanoparticle network was improved because of partial elimination of the insulating ligand shell. Then, an alternative way for further improving the nanoparticle network connectivity was obtained by mixing QDs and nanorods together. The addition of QDs was found to reduce nanorod-nanorod horizontal aggregation, improving electron transport in the vertical direction. Devices based on a QD:nanorod mixture exhibited a higher efficiency than QD-only or nanorod-only devices, reaching the best PCE

of 2.8 %. The size of QDs also affected efficiency: the best device fabricated from PCPDTBT and acid treated large CdSe QDs exhibited a PCE of 3.1 % (Jsc ~8.6 mA cm^{-2}, Voc ~0.63 V and FF ~0.56), higher than previously reported results for the devices based on PCPDTBT and smaller CdS QDs (4.7 nm), which achieved a PCE of 2.7 % [44]. This was attributed to the formation of an improved connection of the inorganic network provided by larger-sized QDs. Similar results were found by other authors [46].

In the same year, Fu et al. [47] used n-butanethiol to remove the oleic acid chains on the nanocrystal surface and achieved a PCE of up to 3.09 % (Jsc of ~7.91 mA cm^{-2}, Voc of ~0.68 V and FF of ~0.56) for P3HT:CdSe devices. In 2013, the same group proposed a similar approach, using acetic acid instead of n-butanethiol for the post-deposition treatment of P3HT:CdSe QDs hybrid films [48]. Compared to the device without post-deposition ligand exchange, acetic acid treatment leads to an increase of PCE from 1.37 % to 1.95 %. Acetic acid is not strong enough to replace all of the long-chain ligands, so the EQE values were less than 60 %. When n-butanethiol, a kind of ligand with stronger interactions towards QDs, was used for ligand exchange, the EQE could be elevated to ~ 70 % [48].

The works of Zhou [44,45], Celik [39] and Fu [47] suggest that the route to highly efficient hybrid devices may not necessarily go through the use of complex, branched inorganic structures such as tetrapods. Instead, it can be achieved by a careful manipulation of surface chemistry of the nanoparticle, film morphology and the control of the interface between the polymer and the inorganic material at a molecular level.

Endorsing this expectations is the fact that the current record efficiency of 4.1 % for a hybrid polymer/QD device, reported by Ren et al. [49] in 2011, was obtained for a device prepared with spherical CdS nanoparticles. To achieve this efficiency, the authors used 4.0 nm CdS QDs capped with n-butylamine and P3HT nanowires, and manipulated the solvents used in the processing. For the so-called non grafting process, 1,2-dichlorobenzene was the solvent used for both QDs and P3HT nanowires. In the so-called grafting process, 1D coaxial nanowire structures were formed by first dissolving the P3HT and CdS into 1,2-dichlorobenzene and octane, respectively, and then mixing these two solutions together. Figure 6 shows transmission electron microscopy (TEM) images and absorption and photoluminescence (PL) properties of CdS/P3HT mixtures obtained by using the grafting and non-grafting processes. In the former, phase segregation is minimized and the P3HT/QD interface is maximized, compared to a randomly distributed system. Devices prepared with 80 wt % CdS QDs with non grafting procedure showed an average J_{SC} of 1.9 mA cm^{-2}, V_{OC} of 0.8 V, FF of 0.40 and PCE of 0.6 %. Devices fabricated using the grafting method, followed by ligand exchange processes using ethanedithiol, gave an average J_{SC} of 10.0 mA cm^{-2}, V_{OC} of 1.0 V, FF of 0.32 and PCE of 3.2 %. The best device performance reached J_{SC} of 10.9 mA cm^{-2}, V_{OC} of 1.1 V, FF of 0.35, with the maximum PCE of 4.1 %. The formation of bicontinuous donor/acceptor phases and a well-defined interface in the hybrid photoactive film through grafting and ligand exchange could largely enhance charge separation and transport efficiency.

Insert Fig 6 here

Figure 6. TEM images of P3HT/CdS hybrid films synthesized (a) without grafting and (b) using grafting process by solvent exchange. The inset images show schematic representations of each; the nongrafting and grafting method is used to control the interface between CdS QDs (yellow spheres) and P3HT NWs (purple lines). (c) Optical properties of P3HT/CdS hybrid thin films with 80 wt % CdS; absorbance of the grafting sample and PL spectra of the nongrafted and grafted films. The vibronic absorption feature at 605 nm in the grafted film is clearly resolved, indicating that the crystalline P3HT NWs are preserved after CdS QDs grafting. The PL spectral intensities of the P3HT/CdS grafted hybrid films are significantly quenched, presumably due to the efficient nonradiative channel for charge transfer from P3HT to CdS phase. (d) Current-voltage (J-V) characteristics of P3HT/CdS hybrid solar cells from nongrafting, grafting and the subsequent ligand exchange. Reprinted with permission from [49]. Copyright 2011, American Chemical Society.

A different approach to control the interface and intermixing between polymer and QDs phase was reported by Dixit et al. [50], in 2012. The authors prepared bulk heterojunction devices by combining P3HT with CdSe(ZnS) core-shell QDs, starting from a polymer/QD bilayer structure. The formation of the bulk heterojunction was induced using thermal inter-diffusion. Optimized devices (annealing for 7 min at 120 °C) delivered Jsc of 1.48 mA cm^{-2}, Voc of 0.62 V, FF of 0.45 and PCE of 5.1 % under irradiation of ~ 8.2 mW cm^{-2}. The surface of the films was very smooth, as observed by scanning electron microscopy images (Figure 7), and the authors considered this as evidence for the formation of an intermingled bulk-heterojunction structure of P3HT and QDs. Although only a few images were presented to illustrate this effect, this work opens up another route to assemble polymer/QD devices, passing though the physical control of the intermixing between QDs and the polymer phase.

Insert Fig 7 here

Figure 7. (Right) SEM micrographs for the bilayer P3HT/ CdSe(ZnS) QDs films (a) before and (b) after annealing. (Left) J–V characteristics for the solar cells fabricated using annealed bilayer P3HT/CdSe(ZnS) QD technique for different annealing times. Reprinted with permission from [50]. Copyright 2012, Elsevier.

Thermal treatments (annealing) provide a means to manipulate the morphology. In the classical organic polymer/fullerene devices, thermal annealing is used to promote controlled phase separation and crystallization. In hybrid organic/inorganic devices, annealing can also be used to remove surface ligands weakly bound to the nanoparticle surfaces. Huynh et al. [34] used this procedure and found that heat treatment aided both in the removal of interfacial and excess pyridine, and in bringing nanorods closer together. Therefore, heat-treated devices showed an overall enhancement of the photocurrent compared to devices prior to heating. Another effect commonly observed after thermal annealing is the aggregation of nanoparticles, which can lead to the increase in the size of clusters. Kuo et al. [51] investigated mixtures of CdSe tetrapods and a polymer with low band gap energy, PDTTTPD, comprising 2,5-di(thiophen-2-yl)thieno[3,2-b]thiophene and thieno[3,4-c]pyrrole-4,6-dione

units. It was found that annealing at a temperature of 130 °C for 20 min led to a significant increase in electrical performance: with reference to the as-prepared devices, the Jsc increased from 3.16 to 7.26 mA cm^{-2} and the PCE increased from 1 % to 2.9 %. The removal of surface pyridine led to a reduction in the inter-particle distance and thus an increase in CdSe packing density, which was presumed to lead to improved electron transport. Other authors reported similar effects using thermal annealing [36,52,53,54].

Chemical vapor annealing is another kind of post-film deposition treatment that can be used to tune the morphology. Wu et al. [55] used benzene-1,3-dithiol to treat CdSe nanorods/P3HT hybrid films. Their experimental procedure comprised a combination of solvent annealing while performing thermal annealing on a hot plate. After the treatment, devices delivered a Voc of 0.553 V, Jsc of 9.7 mA cm^{-2}, and PCE of 2.65 %, corresponding to a 66 % increase in photocurrent and a 70 % increase in efficiency. It is expected that during the vapor annealing, benzene-1,3-dithiol molecules diffuse into the blended film and react with the CdSe surface to replace the bulky alkylphosphonic acid residual molecules, changing the aggregation of CdSe nanorods in the film. This work suggests that chemical vapor annealing process can be another route to surface ligand exchange reaction without the sacrifice of solution processability of nanocrystals.

Pb-based chalcogenides

Other metal chalcogenides, not based on cadmium, have also been combined with polymers and tested in hybrid solar cells. The chemical composition of the core QD is also a matter of primary importance in these devices. Changing the metal enables a large manipulation of the optical properties. For example, by changing the size of the QD from 6 to 2 nm, the energy gap can be tuned from 2.6 to 3.1 eV in CdS [56], while for PbS the band gap can be tuned from 0.7 to 1.3 eV by changing the size from to 8 to 4 nm [57].

Insert Fig 8 here

Figure 8. (a) Energy band diagram displaying HOMO and LUMO of possible polymer donor materials, as well as valence and conduction band edge of multiple inorganic acceptors. For the inorganic materials, solid lines represent bulk energy values, whilst dotted lines represent spherical nanoparticles exhibiting quantum confinement (PbS ~2.7 nm and CdS ~4.0 nm). For P3HT and PCPDTBT, energy values reported in two different works are displayed. All energy levels were taken from literature and summarized in the review article by Wright and Uddin[12]. Energy structure of isolated donor and acceptor materials, showing two major types of heterojunction structures: (b) Type I: Nested band alignment, (c) Type II: Staggered band alignment. Adapted and reprinted with permission from [12]. Copyright 2012, Elsevier.

Figure 8 illustrates the energy levels for a series of conjugated polymers and chalcogenide nanoparticles used in hybrid solar cells, summarized in the review of Wright and Uddin [12]. Considering the low band gap and near-IR absorption characteristics of PbS and PbSe, these materials offer the possibility to extend light-harvesting in solar cells. Besides, an EQE greater than 100 % in PbSe/ZnO has been reported for all-inorganic devices, due to multiple exciton generation and extraction [58]. All these characteristics suggest that Pb-based chalcogenides should be promising candidates for application in hybrid devices.

In 2005, Watt et al. [59] combined PbS QDs coated with short-chain amines with MEH-PPV, obtaining efficiencies of 0.7 % and 1.1 % under white light and single wavelength irradiation, respectively. The amine-capped PbS nanocrystals were found to be more efficient than PbS coated with the original oleate ligands. This was attributed to the charge carriers being able to tunnel through the ligand barrier, or to transfer directly from the conjugated polymer to nanoparticle surface sites left free by incomplete ligand exchange process. In the same year, other groups reported the use of PbS QDs ligand exchanged with amines in combination with conjugated polymers but found poor efficiencies [60,61].

In 2006, Cui et al. [62] aimed at harvesting the infrared solar energy by employing 6 nm diameter PbSe QDs stabilized with a capping layer of oleate molecules in a hybrid photovoltaic device with P3HT. A device assembled with ~80 wt% of QD loading in the polymer matrix and annealed at 140 °C for 10 min delivered Jsc of 1.08 mA cm^{-2}, Voc of 0.35 V, FF of 0.37 and PCE of 0.14 %. Although the overall efficiency was poor, it was shown that the infrared response (between 780 nm and 1600 nm) contributes to 33 % of the overall photocurrent. In 2007, Jiang et al. [63] investigated nanocomposites prepared with PbSe nanocrystals of various sizes with either MEH-PPV or P3HT and obtained sizable photovoltaic response in a spectral range from the ultraviolet to the infrared.

It is noteworthy that, for many years of research, the efficiencies obtained for devices based on lead chalcogenides/polymer and traditional conjugated polymers and P3HT, MEH-PPV and MDMO-PPV were much lower than those obtained with cadmium chalcogenides/polymer based devices, even if using annealing, ligand exchange and post-production treatments [64,65,66,67,68,69].

Noone et al. [70] used photoinduced absorption spectroscopy (PIA) to investigate mixtures of PbSe QDs with P3HT or MDMO-PPV. They observed that these systems showed no evidence of long-lived photoinduced charge transfer between PbSe and both polymers. In contrast, mixtures of the same polymers with either [6,6]-phenyl C61-butyric acid methyl ester (PCBM) or CdSe QDs showed signals attributed to long-lived polarons. The results were correlated with the existence of energy transfer, but not long-lived charge transfer, in the case of MDMO-PPV/PbSe mixtures, and to a near complete lack of either charge transfer or energy transfer in the P3HT/PbSe mixtures [70].

The position of the energy levels should be carefully considered for systems containing QDs. As the HOMO and LUMO of nanoparticles vary with the change in band gap energy, the type of alignment with HOMO and LUMO levels of the polymer may also change. The alignment of energy levels may lead to situations where hole injection or electron injection is either favoured or hindered. Figure 8b,c illustrates type I and type II heterojunction interfaces that may be formed at the polymer/QD interface, according to the size and chemical

composition of the inorganic nanoparticles. The electronic structure of CdSe with several particle sizes forms a type II heterojunction with most conjugated polymers, which has cascading energy levels, with appropriate energy level offsets to facilitate charge separation and transport. Pb-based chalcogenide presents a different behaviour. For example, the energy levels of oleic acid-capped PbS QDs were estimated by Itskos et al. [71] with cyclic voltammetry. Type II heterostructures suitable for light-harvesting devices (i.e., the energetics allow electron and hole photoinduced transfer) are expected to be formed for QD sizes smaller than ~ 4 nm, with a transition to type I band alignment observed for larger QDs. For the smallest investigated QDs of ca. 3 nm, an almost complete quenching of the emission indicates the presence of efficient hole transfer to the polymer despite the use of insulating capping ligands. In light of this particularity, Pb-based chalcogenide nanoparticles have been more effectively combined with low band gap polymers. A better energy-level alignment with these materials, an improved morphology, and higher hole mobilities, leading to a better electron–hole transport balance, are responsible for a more successful combination of Pb-based QDs and low band gap polymers.

In 2010, Noone et al. [72] utilized butyl amine-capped PbS QDs (~3 nm diameter) as IR sensitizers in mixtures with three conjugated copolymers as host materials: PDTPQx (poly(2,3-didecyl-quinoxaline-5,8-diyl-alt-Noctyldithieno[3,2-b:2′,3′-d]pyrrole)), PDTPPPz (poly(2,3-didecyl-pyrido[3,4-b]pyrazine-5,8-diyl-alt-N-dodecyldithieno[3,2-b:2′,3′-d] pyrrole)), and PDTPBT (poly(2,6-bis(3-n-dodecylthiophen-2-yl)-alt-N-dodecyldithieno[3,2-b:2′,3′-d]pyrrole)). These polymers were initially selected because their energy levels allowed the formation of type-II heterojunctions with PbS. Devices were made from 9:1 weight ratios (~ 65 % by volume) of inorganic materials. It was observed that the EQE of the PDTPQx/PbS device was approximately 2 orders of magnitude larger than that obtained using PDTPBT or PDTPPPz, consistent with the formation of long-lived polarons observed with PIA only for the PDTPQx/PbS film. This device delivered Jsc of 4.2 mA cm^{-2}, Voc of 380 mV, FF of 34 % and a PCE of ~ 0.55 %. According to the authors, this corresponds to a ~100 times more photocurrent than devices made from polymers such as P3HT and alkoxy-PPV that were made and tested under identical conditions.

In 2011, Seo et al. [73] combined PDTPBT (poly(2,6-(N -(1-octylnonyl)dithieno[3,2-b:20,30-d]pyrrole)-alt-4,7-(2,1,3-benzothiadiazole)) with oleic acid-capped PbS QDs (first excitonic peak of 1.35 eV). Post-deposition ligand exchange using 1,2-ethanedithiol was applied to the hybrid film. The device with PDTPBT:PbS (10:90 wt%) exhibited a Jsc of 13.6 mA cm^{-2}, Voc of 0.36 V, and a FF of 43 %; resulting in an overall PCE of 2.07 %. The insertion of a TiO_2 layer between the active layer and metal electrode resulted in additional improvement in Jsc (increase of 9.2 %) and FF (increase of 14.5 %), yielding a PCE of 2.70 %. The optimum performance was achieved with a hybrid device using PbS QDs with the first excitonic peak at 795 nm (Jsc of 13.06 mA cm^{-2}, Voc of 0.57, FF of 0.51 and PCE of 3.78 %). This system showed increased Voc in comparison to devices assembled with larger nanoparticles.

In 2012, Zhang et al. [74] employed a bilayer configuration in an inverted device structure (ITO/ZnO/PbS/polymer/MoOx/Ag). PbS QDs of two different sizes were used, with the first excitonic peaks at 1020 and 810 nm and the surface ligands were replaced with 1,3-benzenedithiol by post-deposition treatment, in combination with two polymers, PCDTBT and PCPDTTBTT, which originated a type I and a type II heterojunctions, respectively. A PbS-only device (the polymer layer is absent) was used as a reference, with a PCE of 1.89 % (Voc of 0.41 V, Jsc of 10.35 mA cm^{-2}, and FF of 0.44). After inserting a 15 nm-thick PCPDTTBTT layer, the PCE reached 4.22 %, with improvement of all photovoltaic parameters (Voc of 0.63 V, Jsc of 12.99 mA cm^{-2}, and FF of 0.52). In contrast to PCPDTTBTT, the insertion of a 21 nm-thick PCDTBT layer severely reduced Jsc and FF to 2.54 mA cm^{-2} and 0.11 respectively, and the resulting device exhibited a poor PCE of 0.20 %, despite a high Voc of 0.69 V. The EQE spectra of polymer/PbS devices presented in Figure 9 closely resemble that of the PbS-only device, with a peak at 1050 nm corresponding to the first excited state of the PbS QDs, revealing the vast contribution from the PbS layer to the photocurrent.

Insert Fig 9 here

Figure 9. (a) EQE spectra of solar cells fabricated with a planar junction configuration in an inverted device structure (ITO/ZnO/PbS/polymer/MoOx/Ag), using PbS QDs (NQD1) without polymer, and with a layer of PCPDTTBTT or PCDTBT, which originates a type II and a type I heterojunction with PbS, respectively. (b) J–V characteristics of devices under irradiation of 100 mW cm^{-2}. Reprinted with permission from [74]. Copyright 2012, Elsevier.

In 2012, Piliego et al [75] combined PbS nanocrystals and the narrow band gap polymer PDPPTPT, poly[{2,5-bis(2-hexyldecyl)-2,3,5,6-tetrahydro-3,6-dioxopyrrolo[3,4-c]pyrrole-1,4-diyl}-alt-{[2,2′-(1,4-phenylene)bis-thiophene]-5,5′-diyl}]. The optimized device (PDPPTPT:PbS 10 : 90 wt%; post-treatment with 1,4-benzenedithiol) delivered a Jsc of 12.5 mA cm^{-2}, a Voc of 0.47 V, a FF 49 % and an overall PCE of 2.9 %.

In 2013, Nam et al. [76] presented hybrid solar cells with high efficiency utilizing a novel donor–acceptor combination of PSBTBT (poly[2,6-(4,4′-bis-(2-ethylhexyl)dithieno[3,2-b:2′,3′-d]silole)-alt-4,7(2,1,3-benzothiadiazole)]) and mixtures of PbS_xSe_{1-x} QDs and nanorods. The mean diameter of the spherical QDs was ~ 4 nm, and the nanorods had similar diameters of ~ 4 nm, with an elongated length of 30–40 nm, with optical bandgaps of 1.1 eV and 0.8 eV, respectively. A PCE of ~ 3.4 % was achieved for the optimized device, with a $PbS_{0.7}Se_{0.3}$ QD:nanorod ratio of 0.3:0.7 wt/wt, attributed to the broad-range absorption of light and the efficient charge separation, and by the efficient transport of electrons via straight pathways within nanorods that are continuously interconnected by QDs.

In the same year, Colbert et al. [77] provided spectroscopic evidence that hole transfer produces long-lived charges in PbS/PDTPQx-HD (poly(2,3-bis(2-(hexyldecyl) quinoxaline-5,8-diyl-alt-N-(2-hexyldecyl)dithieno[3,2-b:2′,3′-d]pyrrole) films. For that purpose, PbS QDs were first solution-phase halide-treated with tetrabutylammonium iodide, and then PDTPQx-HD/PbS (1:9 w/w) films were treated with a solution of 3-mercaptopropionic acid. Devices with the structure ITO/ZnO/active layer/MoOx/Ag achieved an EQE of 15 %. The spectrum showed contributions from both polymer and quantum dot materials, but were higher for photons absorbed in the visible rather than those in the infrared.

An overall comparison of the later results obtained using low band gap polymers with previous published works combining Pb-based chalcogenide nanoparicles with more traditional conjugated polymers (i.e., P3HT, MDMO-PPV, etc) indicates that the .energy level alignment is the crucial parameter to achieve more efficient energy conversion in these systems. However, in spite of the significant improvements of hybrid polymer/Pb-based chalcogenide nanoparticles obtained by the combination of QDs with low band gap polymers, so far PbS QDs seem to be more promising for application in thin-film, all-inorganic devices, combined with a metal oxide layer [78,79].

Other metal chalcogenides

Other metal chalcogenides have also been considered as potential candidates for hybrid polymer/QD devices. Since devices based on heavy metals (Cd and Pb) might suffer from environmental safety issues, some efforts have been done to develop technologies based on more environmentally friendly QDs.

Recent efforts involve the combination of SnS [80], FeS_2 [81,82,83] and Sb_2S_3 [84,85] nanoparticles with MEH-PPV, MDMO-PPV or P3HT, but the efficiencies are not yet comparable to those achieved by Cd- and Pb-based devices.

It has been demonstrated that pyrite (FeS_2) is more attractive in terms of cost and availability than other materials[86]. This material has been considered for photovoltaic applications in light of its large optical absorption coefficient and increased light absorption in the near infrared region, due to an indirect band gap of ~0.95 eV [87]. These features should attract interest to the development of devices based on this compound, even though no high performance device has been made yet based on this material. So far, it has been suggested that sulfur vacancies and phase impurities might be related to low PCE values provided by FeS_2 QDs. Those phase impurities might be associated to poor Voc values, even at low concentrations [87]. In spite of having suitable optical properties and being more environmentally friendly, the electrical properties of these QDs might be difficult to control properly due to the formation of surface defects arising from sulfur vacancies. A better understanding of crystal surface and grain boundary properties is pointed out as necessary to improve Voc and PCE [82].

Multinary metal chalcogenide QDs, including those based on I-III-V semiconductors and alloys have also been considered for hybrid polymer/QD devices. Examples using hybrid solar cells based on multinary nanocrystals have been reported for $CuInS_2$ [88,89,90,91,92,93,94] and $CuInSe_2$ [95] combined with a variety of conjugated polymers.

There is a huge interest in using this type of material. $CuInS_2$, for example, has a small direct band gap of 1.5 eV, a large absorption coefficient and a low toxicity. Moreover, this material may be prepared by a range of colloidal synthesis methods with different morphologies and different crystal structures [96]. Readers interested in additional information on the synthesis of multinary metal chalcogenide nanocrystals, their properties and applications, should be directed to an excellent review published elsewhere [97].

The first attempt to use $CuInS_2$ nanoparticles embedded into a conductive polymer (poly(3,4-ethylenedioxythiophene: poly(styrene sulfonic acid) was demonstrated by Arici et al. [88] in 2003, but the solar cells provided PCEs below 0.1%. For a long time there was no much improvement in devices assembled with such kind of QDs and it was only recently that significant progress has been made. Remarkable efficiencies of up to 1.7 % [93] and 2.8 % [91] were reported for polymer/$CuInS_2$ QDs hybrid solar cells by taking advantage of *in situ* synthesis routes, and the use of copper and indium xanthates as precursors that decompose in the polymer matrix during thermal treatment.

The influence of pyridine, alkylamine, and hexanethiol as capping ligands on the morphology of the active layer and the electrical characteristics of solar cells based on elongated and pyramidal $CuInS_2$ nanocrystals mixed with P3HT were recently demonstrated [92]. It was found that the morphology and a suitable choice of capping ligands are not the only limiting factors in the system. Whereas alkylamines were found to be an unsuitable choice of ligands, the application of a ligand exchange procedure with hexanethiol was found to have a favorable impact on the morphology, resulting in an enhancement of the rectification ratio of the device. Nevertheless, a low performance was achieved in comparison to solar cells based on other colloidal semiconductor nanoparticles. According to cyclic voltammetry measurements, an unsuitable alignment of the energy levels for $CuInS_2$ nanocrystals and P3HT was observed, which probably makes the charge transfer process rather inefficient in this system [92]. Thus, the alignment of energy levels is considered a critical issue for polymer/$CuInS_2$ solar cells.

It is worth mentioning that all these alternative materials have been much less explored so far than Cd- and Pb-based chalcogenides. Nevertheless, it is expected that further investigations will continue on this research topic, on the pursuit of more environmentally friendly devices. Despite differences in terms of optical and electrical properties associated with chemical composition, other drawbacks are usually associated with the use of QDs: surface chemistry issues (presence of traps, defects, etc), need of bulk capping molecules, adjustment of nanoscale morphology and phase separation of hybrid active layers. Further development of technologies based on other kinds of chalcogenide nanoparticles, thus, might involve the use of some of the

strategies already applied for Pb and Cd systems. Furtheremore, due to different electronic properties of these novel compounds, other families of polymers should also be investigated in order to achieve the desired energy level alignment of organic and inorganic semiconductors.

Persistent difficulties associated with polymer/QD systems

It is difficult to point out which is the most important effect or property related to polymer/QD solar cells that could originate devices with efficiency close to polymer/fullerene devices. Chemical composition, size, shape and structural quality of nanoparticles directly influence the performance of the devices [46,98]. It was demonstrated that even the type of solvent used in the purification steps after the synthesis can affect the ligand shell composition of CdSe and PbSe QDs, thus affecting their properties, such as luminescence [99]. However, even with the best materials in hands, it is not straightforward that the resulting hybrid mixture will originate a film with high quality (in terms of morphology, defects, thickness, etc). Parameters related to processing conditions, such as the solvent employed during film deposition and post-production treatments are also crucial.

Since there are many parameters affecting device performance, it becomes extremely case sensitive. As a consequence, efficiencies reported for hybrid solar cells vary largely among different research groups, even if they are using similar approaches. Direct comparison between different works might be tricky thus. Furthermore, efficiencies have not improved significantly over the past 10 years, from ca. 1.7 % back in 2002 and kept close to 3-4 % to date. These values are much lower than the efficiencies obtained for all-inorganic solar cells based on PbS/ZnO (~ 7 % [79]) or organic solar cells (~ 10 % [100]). In a recent review, Saunders [10] pointed out that the best PCE value for a polymer/nanoparticle solar cell was 3.2 % in 2010, only 0.4 % higher than the second best value of 2.8 % reported in 2005. He stated that this represents a modest PCE increase (of about 0.1 % per year), which contrasts with PCE increase for polymer solar cells within the same period (2.4 % in 2005, ca. 0.5 % per year) [10]. When analyzing these data one should remember that, despite the recent popularity of polymer/QD systems, the number of research groups working on the development of polymer/fullerene devices is still much larger than those working on hybrid polymer/QD devices.

The different behaviour between polymer/fullerene and polymer/QD systems results, in part, from the different nature of organic and inorganic materials. In the bulk heterojuction approach, an intimate contact is desired and, in the case of polymer/inorganic nanoparticles mixtures, scientists are manipulating two components which usually do not easily interact. Morphology control and optimization in polymer/fullerene devices by thermal annealing and treatments with small thiol molecules, for example, occur because relatively small PCBM acceptors diffuse into amorphous P3HT domains providing more intimate mixing. An equivalent treatment, in terms of morphology control and optimization, has to be identified for bulk heterojunction hybrid devices.

A systematic investigation, careful and thorough exploration of the results obtained so far are extremely necessary for the advance of the field. Efforts to compare and understand, in details, the differences between polymer/QD and polymer/fullerene systems, and how to transfer the improvements obtained in classical organic/organic devices to organic/inorganic ones, are welcome and should be encouraged. Figure 10 shows a comparison between P3HT/PCBM, P3HT/polymer, and P3HT/CdSe based solar cells provided by Li et al. [101]. Clearly, these systems show different behaviours and the P3HT/PCBM device is by far the most efficient one, with much higher values of Jsc and FF. An investigation with transient photocurrent and photovoltage measurements showed that there are fundamental differences in the nature of charge collection. Polymer/QDs and polymer/polymer devices exhibit much more pronounced charge trapping compared to polymer/fullerene devices. For these two systems, detrapping of charge is much slower, and field-dependent detrapping is observed for the P3HT/CdSe system. Besides, the shape of the current-voltage curves from these devices is influenced by trapping phenomena. The authors suggested that traps in the CdSe phase might be mainly associated with nanocrystral surface and, therefore, improvements in device efficiency previously reported by the use of nanorods and tetrapods could be explained by the lower relative surface area of these kinds of particle geometries compared to dots.

Insert Fig 10 here

Figure 10. (a) External quantum efficiency (EQE) and (b) current–voltage characteristics under 100 mW cm^{-2} illumination for P3HT/PCBM (squares), P3HT/CdSe (circles), and P3HT/F8TBT (poly((9,9-dioctylfluorene)-2,7-diyl-alt-[4,7-bis(3-hexylthien-5-yl)-2,1,3-benzothiadiazole]-2,2-diyl)) (triangles) devices. Reprinted with permission from reference [101]. Copyright 2011, Willey-VCH Verlag GmbH & Co.

Noone et al. [102] used quasi-steady-state photoinduced PIA to study the dynamics of polymer polarons formed via photoinduced electron transfer from the polymers P3HT, MDMO-PPV and PDTPQx-HD, combined with a series of acceptors, including PCBM, ~3.5 nm CdSe (treated with pyridine), ~3 nm PbS QDs (treated with butylamine), ZnO nanonetworks, and mesoporous TiO_2 films. Regardless of the polymer used, photoinduced electron transfer to all inorganic acceptors yielded longer lived polarons compared to photoinduced electron transfer to PCBM. The possible explanations for these differences were assigned to (i) increased charge screening by the higher dielectric constants of inorganic materials, slowing recombination and thus resulting in the longer observed lifetimes; or (ii) charge trapping by surface states arising from inorganic materials. Inorganic acceptors are likely to possess a much higher abundance of traps in light of surface or defect states. To test the hypothesis if trap states were associated with unpassivated surfaces from inorganic nanoparticles, the authors prepared PDTPQx-HD/PbS active

layers and treated them with 1,2-ethanedithiol. The device with untreated active layer had Jsc of 0.17 mA cm^{-2}, Voc of 0.47 V, FF of 0.30 and PCE of 0.02 %. Treating the active layer with 1,2-ethanedithiol decreased Voc to 0.40 V and increased Jsc to 2.1 mA cm^{-2} and FF to 0.33 %, resulting in an overall increase of PCE to 0.25 %. The increase in Jsc upon ligand treatment and the change in polaron lifetime are consistent with the hypothesis that thiols are passivating deep traps on the surface of QDs, resulting in an increased mobility and decreased recombination loss, both of which could improve the efficiency of photogenerated charge collection in hybrid systems.

Heinemann et al. [103] employed stationary PIA and light-induced electron spin resonance (LESR) measurements to make a comparative study of P3HT/CdSe and P3HT/PCBM films. CdSe nanocrystals with an average diameter of 3.0 nm and ligand exchanged with pyridine were used in that work. Charge transfer was observed in both systems, although the photoluminescence quenching yield was lower for the hybrid system (~ 70 % and ~ 95 % relative to the photoluminescence intensity of the neat P3HT sample for the P3HT/CdSe and P3HT/PCBM samples, respectively). The recombination kinetics revealed by PIA supports a model in which only shallow traps exist in the PCBM-based sample, whereas a larger amount of deeper trap states seems to be present in the case of the nanocrystal-based composite. It was also concluded that the nanocrystals have significant impact on the polymer chain conformation, as well as on the freedom to form extended aggregates of polymer lamellae. LESR measurements showed that the nanocrystals induce more pronounced disorder in the polymer phase and, as a consequence, it induces the formation of localized states and energetic disorder in this phase. The limiting factors in photovoltaic blends of P3HT:CdSe were attributed to non-appropriate morphology of the thin films and structural and energetic disorder.

Due to the poor interaction between polymers and inorganic materials, phase separation is a frequently observed phenomenon in polymer/nanoparticle hybrid systems, and might lead to the formation of nanomorphologies wherein nanoparticles are organized as "islands", dispersed in a polymer "sea". Crystallization, interchain interaction and phase separation of active layers depend on the concentration of composite mixture and its loading amount [104,105]. Phase separation and aggregation of nanoparticles were reported to increase with CdSe loading amount [104,105]. However, monotonic increase of efficiency and Jsc with the increase of CdSe/P3HT loading amount was also reported [105]. In fact, for polymer/CdSe mixtures, the best photovoltaic responses are obtained when ~ 80-90 wt % of nanoparticles are incorporated into the polymer matrix [29,106,107,108,145]. This arises from the nature of charge transport in the CdSe phase. The high loading is a necessary condition for achieving a percolation network in the inorganic phase.

There is a fine line in the balance between increasing nanoparticle loading to enhance connectivity and charge transport, while still keeping, to a controlled extent, phase separation in the polymer matrix. Ideally, the formation of a percolation network of nanoparticles at high loadings would be possible without phase segregation. However, the phase segregation phenomenon increases as the contact area between the aggregating particles increases. Thus, any effort that contributes to increase the solubility/miscibility of organic and inorganic counterparts is encouraged. For example, Liu et al. [109] compared the morphology and device performance of composites of CdSe nanorods (~7 nm in diameter and 30 nm in length, ligand exchanged with pyridine) and P3HT polymers containing different end-groups (NH_2 or Br). Figure 11 presents the TEM images of the films containing different loadings of nanorods. The TEM images of CdSe/P3HT-NH_2 composites suggested a high degree of homogeneity. In contrast, CdSe/P3HT-Br composites prepared under the same processing conditions exhibited significant phase segregation, suggesting poor dispersion of the nanocrystals in the polymer. The authors speculated that P3HT-NH_2 partially replaces the pyridine on the surface of the nanorods through coordination of its amino end-group with the CdSe, and thereby enhancing the miscibility of the polymer with the nanocrystals. Devices assembled with P3HT-NH_2 exhibited higher PCE values than those devices made by using P3HT-Br. This was explained by the larger interfacial area for exciton charge separation due to the good dispersion of CdSe in P3HT-NH_2 matrix. Although these films had much enhanced nanoparticle dispersion, the highest PCE achieved was 1.6 %.

Insert Fig 11 here

Figure 11. TEM images of composites consisting of CdSe (20 wt %)/P3HT-Br (top left), CdSe (20 wt %)/P3HT-NH_2 (top right), CdSe (40 wt %)/P3HT-Br (bottom left), and CdSe (40 wt %)/P3HT-NH_2 (bottom right), respectively. The functional end-group in P3HT-NH_2 reduces the aggregation of CdSe nanorods in the composites. Reprinted with permission from reference [109]. Copyright 2004, American Chemical Society.

As an alternative, some authors suggested not trying to avoid aggregation, but to trigger it in controlled ways. Rhodes et al. [110] proposed directing nanoparticle aggregation intentionally by using 1,2-ethanedithiol, which is known to bridge deposited nanoparticles. They studied the triggerered aggregation of PbS/polymer dispersions prior to film formation by spin-casting and observed that small aggregates or micrometer-sized crystals formed depending on the concentration of 1,2-ethanedithiol.

It is clear that morphology plays a key role in the route to achieve high efficiencies. However, there are other parameters to be considered, as optimization of morphology alone might not be enough to produce hybrid polymer/QD devices with efficiencies similar to those achieved for polymer/fullerene devices. The presence of traps on the nanoparticle surface, either by incomplete ligand coverage or by oxidation, can also affect charge generation and charge transport, increasing charge recombination therefore.

Dowland et al. [111] combined the morphology information with transient absorption spectroscopy (TAS) data to correlate charge generation with morphology. Firstly it was demonstrated that the nanomorphology may be controlled by altering the relative amounts of active layer components in CdS:P3HT films

prepared by the *in situ* decomposition of a xanthate precursor of CdS. As the CdS loading is increased, the P3HT domain size is reduced, making the migration of excitons formed within the polymer more likely to reach an interface, thus increasing charge generation yield. A greater CdS content may also result in a more crystalline character and a higher degree of interconnectivity within the CdS domains, which may lead to a more facile electron transfer process. Furthermore, charge generation from a hole transfer process appears to be a substantial contributor to the device photocurrent. On the other hand, photocurrent extraction required for good photovoltaic devices relies on larger and/or more crystalline P3HT domains. Thus, films with higher CdS content having smaller, less crystalline P3HT domains, lead to a better charge generation, but worse photocurrent extraction. It was also shown that charge generation from P3HT excitons is heavily dependent on nanomorphology, while charge generation through hole transfer from CdS is largely unaffected by the morphology, which implies that the diffusion length of photogenerated CdS holes must be greater than the CdS domain size across all compositions studied. Charges generated from excitation of CdS accounted for approximately 50% of the Jsc under AM 1.5 illumination.

Cappel et al. [112] recently demonstrated the charge generation dynamics in CdS:P3HT films prepared by the *in situ* decomposition of a xanthate precursor of CdS with TAS. In order to excite mostly the CdS, the authors irradiated the sample with an excitation wavelength of 355 nm, and to excite solely P3HT, an excitation wavelength of 550 nm was used. It was observed that the charge generation via hole transfer from CdS to P3HT is more efficient than charge generation from P3HT to CdS. Furthermore, the lifetimes of charges in CdS were found to be much longer than the lifetimes of excitons in P3HT. Thus, charge generation following excitation of the inorganic component is more efficient than charge generation from the organic polymer. Based on this rational, the authors indicated that it is very important to take advantage of such effect as a design pathway for the future development of hybrid solar cells.

Overall, the limiting factors for achieving highly efficient hybrid polymer/QD devices are related to the nanoparticle surface chemistry and the nanomorphology of the photoactive layer. Therefore, many authors have focused on modifying nanoparticle surface, aiming at improving the polymer/QD interface, obtaining better dispersions of these QDs in the polymer matrix and tuning morphology. In the next section, approaches that directly influence device efficiency via manipulation of surface chemistry of QDs will be explored.

Manipulation of the QD surface via ligand exchange

Capping ligands (or passivating ligands) play a crucial role in QD chemistry and physics. During the synthesis, among other factors, they are responsible for maintaining the stability and limiting size growth. A description of the role of ligands in the synthetic process was reviewed by Yin and Alivisatos [113]. After the synthesis, considering the application in optoeletronic devices, ligands play a crucial role in the passivation of surface defects, such as dangling selenide bonds, that behave as charge carrier trap sites, and therefore have been associated with decreased device performance. Capping ligands also allow for the manipulation of the QDs dispersion in different solvents, and their incorporation into different polymer matrices. Detailed reviews about the role of surface ligands can be also found elsewhere [114,115].

To manipulate the surface, one method often used is the ligand exchange, in which the original ligands used during synthesis are then replaced by the ligand of choice. This is a powerful tool to tune the properties of nanoparticles, and to make QDs amenable to certain chemical reactions. For example, the exchange of trioctylphosphine oxide (TOPO) and dodecylamine with 3-mercaptopropionic acid quenches the band edge emission and enhances deep trap emission [116], while exchanging with 1,2-ethanedithiol or 1,2-ethanediamine significantly improves exciton dissociation yield and/or charge carrier mobility [117]. This process can also give QDs solubility in hydrophilic and polar solvents, such as water.

Typically, a functional group with a high affinity for binding to the surface of QDs (such as sulfur or nitrogen), a spacer group (such as an alkyl or aryl chain), and a functional group or chain that possesses the chemical property of interest are employed in the molecule to be used in the ligand exchange process.

Pyridine has been widely accepted as capping ligand for cadmium chalcogenide QDs. This molecule has a greater affinity for the CdSe surface, and therefore can easily replace bulky surfactants usually employed in the QD synthesis. The advantage of pyridine is that the smaller radius of this molecule allows a better interaction between the QDs and the polymer chains, facilitating charge transfer and thus, leading to devices with higher efficiencies [118,119]. On the other hand, some authors observed that the use of pyridine leads to the formation of CdSe agglomerates, which may damage film morphology [40].

Lokteva et al. [120] reported the impact of single and multiple pyridine treatments on oleic acid-capped CdSe nanoparticles properties. Interestingly, repeated pyridine treatment was found to lead to a more complete ligand exchange, which in turn enabled more efficient charge transfer, but at the same time the performance of the solar cells was reduced. The authors correlated this fact with the increased aggregation tendency of repeatedly pyridine-treated particles, which negatively influenced the morphology, as well as with a larger amount of surface defects in particles stabilized by the pyridine ligand shell.

Alkylamines are another class of materials that have lead to very good device efficiencies [36,121,122], even higher than the more commonly used pyridine [123]. Investigations of the charge carrier generation and recombination processes by LESR obtained from both pyridine- and butylamine-capped CdSe nanoparticles mixed with P3HT elucidated the origin of the photocurrent rise in butylamine-capped CdSe/P3HT hybrid cells. The butylamine treatment led to an improvement of

charge carrier generation, since cadmium dangling bonds, which play the role of deep electron traps, were more efficiently passivated in the case of butylamine (it was suggested that nearly all Cd surface sites are passivated before annealing). Moreover, the use of butylamine instead of pyridine removes the hole traps associated with the pyridine aromatic ring, also improving charge transport across the hybrid film [123].

Thiols and thiophenes are also well explored alternatives as capping ligands [124,125]. Sulfur-based molecules may allow efficient control of the kinetics of QD growth, effective surface passivation, provide stability, water solubility and desirable surface charge and surface functionality to the inorganic QD core. Greaney et al. [126] achieved a power conversion efficiency of 1.9 % for hybrid organic/inorganic solar cells fabricated from mixtures of tert-butylthiol-treated CdSe QDs and P3HT. Compared to devices made from pyridine-treated and non-ligand exchanged CdSe, the thiol-treated CdSe QDs exhibited the highest Jsc and Voc (Figure 12). This was expected since the introduction of small, strongly binding, electron-donating ligands should enable improvement in the open-circuit voltage by raising the LUMO energy level of the nanocrystal acceptor phase, thereby increasing the energy offset from the polymer HOMO.

Insert Fig 12 here

Figure 12. (Left) Cyclic Voltammetry measurements that allow the calculations for the reduction onset values of CdSe(non-ligand exchanged, NL) (1), CdSe(pyridine, Py) (2), and CdSe(tert-butylthiol, tBT) (3): 0.57, 0.50, and 0.66 V, respectively. (Right) Current-voltage curves for devices assembled with ITO/PEDOT:PSS/P3HT:CdSe/Al structure, made with CdSe(NL) (1), CdSe(Py) (2), or CdSe(tBT) (3) nanoparticle acceptors. Reprinted with permission from reference [126].Copyright 2012, American Chemical Society.

Albero et al. [127] investigated the influence of the dipole moment of small molecules (thiol derivatives) anchored to the surface of CdSe over the interfacial charge recombination dynamics in CdSe/P3HT mixtures (Figure 13). According to the authors, the polarizability of the CdSe/P3HT interface is the key to achieve efficient charge separation and slow back electron transfer (recombination), two of the most important processes to boost the photocurrent and voltage of the devices. Besides, the different chemical nature of the dipole molecules has a strong effect over the QD agglomeration and film nanomorphology. Positive effects of dipole molecules as modifiers for interfaces in all-organic solar cells have also been reported by other authors [128,129,130].

Insert Fig 13 here

Figure 13. (Top) Aromatic thiol derivates used to coat the surface of CdSe QDs. The arrows indicate the direction of the dipole at the molecule. The calculated dipole moment is also shown for each molecule. (Bottom) Transient absorption decay measurements for the different films at room temperature (λ_{ex} = 470 nm and λ_{probe} = 980 nm). Reprinted with permission from reference [127] with permission from PCCP Owner Societies.

An alternative approach to manipulate the surface chemistry of QDs involves the shortening of long chain surface groups by thermal cleavage [131], wherein device performance improves because of the reduction of polymer/QDs distance and inter-particle distances, enhancing the charge transport in the inorganic phase.

Capping of the nanoparticle with additional layers of inorganic semiconductor material may also be an important step. These inorganic surface modifications create new hybrid systems with properties which are dependent on both core and shell materials. So far, there have been only a few reports on the application of core-shell QDs in hybrid polymer/QD solar cells [132,133]. For example, a P3HT/ZnTe(ZnSe) hybrid solar cell showed a PCE much higher than that of the P3HT/ZnSe control device or that of the P3HTonly photovoltaic device [133]. Nevertheless, the overall efficiency of polymer/core-shell devices is still very poor. For a polymer/CdSe(ZnS) system, it was demonstrated that hole transfer from the to the polymer is dependent on the shell thickness [134]. The shell might behave sometimes like an insulating medium that limits electronic communication with surface ligands or the environment, which could result in undesirable or unpredictable device performance.

All-inorganic nanoparticles composed of CdSe/ZnS and PbS capped with metal chalcogenide complexes, such as $Sn_2S_6^{4-}$, have been prepared [135]. These types of ligands can be used to increase the solubility of semiconductor nanoparticles in polar media, such as water, formamide and dimethylsulfoxide. Also, it has been shown that inorganic ligands considerably enhanced the inter-dot electronic coupling in QD solids, leading to facile charge separation and transport [136]. After the ligand exchange reactions, the interparticle distance in the QD film gets smaller, facilitating the electron/hole transport.

Particularly interesting was a hybrid passivation scheme recently proposed by Ip et al. [137], aimed at achieving an improvement in the combination of surface passivation and film density. This scheme uses halide anions in the solution phase to bind hard-to-access sites and, at the same time, introduce metal cations to bind unpassivated surface chalcogens, targeting the removal of valence-band-associated trap states. Finally, during the solid-state film-forming process, mercaptopropionic acid is used as a bidentate organic linker to maximize packing. These molecules completely displaced the original long aliphatic ligands that the halide passivants were unable to remove. Using the hybrid passivation approach, the authors assembled a solar cell with an all-inorganic structure with a certified efficiency of 7.0% [137].

While treatment with inorganic ligands has been a regular approach for metal chalcogenide/metal oxide all-inorganic solar cells, this has not been the case for hybrid polymer/QD devices. It would be ideal to have an equivalent procedure during the solution process of hybrid solar cell fabrication. However, it remains a challenge because once the long alkyl chain ligands on the nanoparticle surface are replaced with small molecules, the QDs tend to aggregate and precipitate out from the organic solvent, not being mixed uniformly with the polymer.

Although very functional, ligand exchange has its limitations. Inefficient loading of the ligands onto the QDs and poor long-term stability due to oxidation are among the current problems. The next section deals with novel approaches introduced to eliminate the need of extra ligands on the surfaces of QDs.

Approaches without the use of additional capping molecules

In situ synthesis of QDs

In the pursuit of alternatives to use QDs without robust capping ligands, an elegant approach is the preparation of hybrid polymer/QD films via the synthesis of the inorganic nanoparticles *in situ*. This route is expected to lead to a more favorable interface between the polymer and the QDs for charge transfer, while giving a fine mixed morphology. Reports showing PbSe grown in the presence of PPV-based polymers date back to 2004 and 2005, by Watt and cols. [59,138,139,140].

In 2008, Stavrinadis et al. [141] showed the controlled assembly of PbS nanorods through oriented attachment of PbS nanocrystals synthesized in the presence of MEH-PPV. Lead acetate trihydrate was used as precursor and was reacted with sulfur in the presence of the polymer, in a mixture of dimethylsulphoxide and dichlorobenzene, at temperatures varying between 100 and 178 °C. The composite was precipitated from solution by the rapid addition of alcohols, and the aggregation of the nanocrystals was dependent on the polarity of the alcohol. Using methanol results in an ordered aggregation of nanocrystals into spherical particles, while precipitating with other alcohols, such as ethanol, propanol, or hexanol, results in the formation of nanorods.

In 2009, Liao et al. [142] reported the synthesis of CdS nanorods with various aspect ratios in the presence of head-to-tail P3HT. Cadmium acetate dehydrate and sulfur were used as precursors and the reaction was carried out in a mixture of dimethylsulfoxide and dichlorobenzene, with temperature varying between 120 and 180 °C. The particle geometry and size were controlled by temperature, concentrations of the Cd precursor, or time (Figure 14). Importantly, it was observed that the choice of solvent impacts on the conformation of the P3HT chains. In surfactant-assisted synthesis, nanoparticle growth is controlled by electrostatic interactions and by steric hindrance induced by the surfactant functional group and surfactant side alkyl chains, respectively. P3HT provides a combination of both effects as it contains an electron donating sulfur functionality, a potential anchorage for the nucleation and growth of nanoparticles, along with steric hindrance due to long hexyl side chains. A planar P3HT conformation may provide flat, stacking molecular architecture to guide the growth of CdS nanocrystals in an oriented approach. The aspect ratio of the resulting nanorod could be controlled according to the length scale of the P3HT chain that extended into the diluting environment, which was controlled by a variation of the solvent composition. Devices prepared with these composites showed that both Jsc and FF increased with the aspect ratio of the CdS nanorods, and Voc remained unchanged at ~ 0.64 V, reaching PCE as high as 2.9 %.

Insert Fig 14 here

Figure 14. (Left) Scheme of the synthesis of P3HT/CdS composites by *in situ* synthesis of CdS spherical nanocrystals or nanorods via reaction of cadmium acetate dehydrate and sulfur in the presence of the polymer, dimethylsulfoxide and dichlorobenzene. The Cd^{2+} ions are assumed to be coupled with the unpaired S along the P3HT planar chain network. (Right) Average aspect ratio of CdS nanocrystals plotted as a function of the reaction time for the CdS nanorods growth. Reprinted with permission from [142]. Copyright 2009, American Chemical Society.

In the same year, Dayal et al. [143] employed a mixture of high boiling point solvents, 1-octadecene and 1,2,4-trichlorobenzene for the synthesis of CdSe QDs in a P3HT solution. Dimethylcadmium and sulfur were used as precursors and nanoparticle growth was carried out at 230 ºC. In this case, reaction temperature also played a significant role, affecting the size and size distribution of spherical QD particles. The use of higher temperatures allowed by the high boiling point solvents is expected to yield more homogeneously dispersed CdSe QDs compared to low temperature synthetic procedures.

In 2011, Khan et al. [144] directly synthesized CdTe nanoparticles in the presence of P3HT, using cadmium acetate dihydrate and tellurium powder in trioctylphosphine as precursors. TEM images revealed that the ratio of P3HT to cadmium acetate precursor plays a significant role in controlling the size and shape of the nanocomposites. At low CdTe concentration, the P3HT is expected to have more binding ability, resulting in the formation of some nanorod-shapped particles. As the CdTe concentration increases, precipitation of nanoparticles is observed. The optimum condition was considered to happen when both effects are suppressed. An enhancement in current density was observed for a bulk heterojunction device of P3HT/CdTe nanocomposites combined with PCBM.

In 2013, Peng et al. [53] employed P3HT as the ligand to synthesize P3HT-capped CdSe superstructures in a mixed solution of 1,2,4-trichlorobenzene and dimethyl sulfoxide. This synthetic procedure yielded homogeneous CdSe superstructures that were constructed by 5 nm- to 10 nm-sized CdSe nanoparticles. The solar cell exhibited Voc of 0.54 V, Jsc of 4.25 mA cm^{-2}, FF of 57.5 % and PCE of 1.32 %.

An alternative approach to the *in situ* synthesis of QDs in a polymer solution is the *in situ* synthesis of the QDs in a polymer film. This approach is performed by the deposition of films from polymer solutions which contain a soluble precursor of the inorganic nanoparticles, followed by the reaction to form the nanoparticles in the pre-deposited film.

In 2010, Leventis et al. [145] reported the fabrication of CdS/P3HT films based on the controlled *in situ* low temperature thermal decomposition of a metal xanthate precursor in the polymer film. Different CdS:P3HT ratios were investigated and TAS measurements revealed that similar yields of charge separation per absorbed photon are observed with the use of a 4.7:1 CdS:P3HT weight ratio as those

achieved for a PCBM:P3HT system. Photovoltaic devices based upon these nanocomposites showed PCE of 0.7 % under full AM1.5 illumination and 1.2 % under 10 % incident power illumination [145]. In 2011, the same group [146] showed that the nanomorphology of such CdS/P3HT films is strongly dependent upon the annealing temperature. TAS studies supported this observation, indicating high yield of charge photogeneration after annealing. The photovoltaic performance presented the same dependency. Optimized devices containing such hybrid layers, with the configuration glass/ITO/TiO_2/CdS (interface layer)/CdS/P3HT(active layer)/PEDOT:PSS/Au and annealed at 160 °C, delivered a Jsc of 4.8 mA cm^{-2}, Voc of 0.84 mV, FF of 53 % and efficiency of 2.17 % [146] (Figure 15). In this device architecture, the role of the CdS interface layer was not investigated in details, but the authors suggest that it helps to reduce the direct recombination between photogenerated hole in the P3HT and the electrons at the TiO_2/ITO electrode, leading to a substantial improvement of efficiency compared to the device prepared with a similar architecture, but without the CdS layer (PCE increased from 1.45 % to 2.17 %, see devices (iii) and (iv) in Figure 15).

Insert Fig 15 here

Figure 15. (a) Devices architectures and (b) current-voltage characteristics of CdS/P3HT solar cells. Devices (i), (ii), and (iii) employed CdS/P3HT films that were annealed at 105, 120, and 160 °C, respectively. Devices (i)–(iii) were fabricated using device Architecture A. Device (iv) was fabricated using Architecture B and employed a CdS/P3HT photoactive layer that was annealed at 160 ° C. Reprinted with permission from reference [146]. Copyright 2011, Willey-VCH Verlag GmbH & Co.

In 2012, Reynolds et al. [147] compared the properties of the *in situ* grown CdS QDs and P3HT/CdS hybrid films obtained via this method with regular, as-synthesized P3HT/QD films containing equivalent amounts of CdS (approximately 65 wt.% QDs). The regular QDs used were capped either with oleic acid or with hexylamine. The authors observed that the in situ grown CdS forms a nanostructured, interconnected layer which should provide a larger number of percolation pathways for improved charge collection and may be considered as an un-capped, interconnected network of branched nanoparticles. In contrast, both the oleic acid and hexylamine capped QDs are seen to stay within the P3HT matrix as discrete, un-aggregated dots, although the shorter hexylamine ligand appears to allow the inorganic components to sit closer together. Comparing the morphology information with TAS data (Figure 16) the authors concluded that a hybrid polymer/inorganic system in which the inorganic acceptor is grown essentially "ligand-free" *in situ* is better at dissociating excitons into free charges than a system in which the inorganic acceptor is in the form of pre-synthesized QDs with capping ligands, even after these ligands have been exchanged to facilitate efficient electron transfer and charge transport [147].

This kind of approach has been extended to the design of polymer/$CuInS_2$ [91,93] and polymer/Sb2S3 nanocomposites [84] and to deposit nanocrystalline ZnS thin films hosting CdSe–CdS–ZnS QDs [148], indicating that the in-situ thermal decomposition of single-source precursors is an attractive and versatile route to hybrid inorganic–organic optoelectronic devices, and might be applicable to other metal chalcogenides as well.

Insert Fig 16 here

Figure 16. (Top) TEM images of equivalently loaded P3HT/CdS misxtures: a) oleic-capped CdS QDs, b) hexylamine-capped CdS QDs, c) *in situ* grown CdS. Darker regions are the inorganic component. Scale bars are 50 nm. (Bottom) Transient absorption decays for films of pristine P3HT (black), P3HT/CdS QDs with oleic acid (red) or hexylamine (green) capping ligands, and two P3HT/*in situ* grown CdS films of different ratios (blue and magenta). Excitation was set at 550 nm and 60 mJ cm^{-2} and the absorption was probed at 980 nm. Inset: transient absorption spectrum at 10 ms for a P3HT/*in situ* grown CdS film (blue) and for a P3HT/hexylamine QD film (green) showing a ground state bleach and the $P3HT^+$ polaron peak. Reprinted with permission from reference [147]. Copyright 212, Royal Society of Chemistry.

Pre-assembled, interconnected QD networks

Another sophisticated approach, which has hardly been explored, is the use of chalcogenide-based aerogels. In the aerogel, the nanoparticles are "connected" together through S-S or Se-Se bonds, forming an electrically integrated network, which can improve electron hopping in this phase. Such architectures are of interest for applications requiring maximal transport of charge (through the gel network), also maintaining an interconnected pore network.

Chalcogenide sol-gel methods have been used to assemble II-VI and IV-VI nanoparticles into mesoporous colloidal networks with inorganic particle interfaces that do not present the barriers to electrical transport, yet remain quantum-confined [149,150]. Figure 17 schematically represents the sol-gel transformation of CdSe quantum dots, initiated by oxidation of surface thiolate ligands, for example. Removal of surface groups is followed by the solvation of Cd^{2+} ions, exposing Se^{2-} on the surface. This material undergoes further oxidation, giving diselenide or polyselenide species, which link the nanoparticles together and form a gel network. Supercritical drying allows the porosity to be maintained, yielding an aerogel [150].

Insert Fig 17 here

Figure 17. Scheme and associated TEM micrographs showing the gel formation, via a viscous sol, of metal chalcogenide nanoparticles that are surface-capped with thiolates (RS-). Upon introduction of an oxidant, disulfides are formed (RS–SR), providing open sites on the particle surface for assembly into oligomers and eventually polymers (gels). Representative thiols (RS–H) and oxidants are also illustrated. The micrographs are of CdSe materials [prepared with ca. 3 nm spherical particles using MUA for capping and tetranitromethane (TNM) for oxidation, with the bar corresponding to 100, 20, and 20 nm, respectively, from left to right. Reprinted with permission from reference [150]. Copyright 2007, American Chemical Society.

In 2012, De Freitas et al. [151] reported, for the first time, an investigation of mixtures of CdSe(ZnS) core-shell aerogels and P3HT nanocomposites using photoelectrochemistry measurements and TAS. Different ratios of aerogels were mixed with P3HT and the properties of the resulting composites were compared to those of composites obtained using regular CdSe(ZnS) core-shell QDs. The systems containing P3HT:aerogel and P3HT:QDs behave differently as the

concentration of the inorganic material increases, as shown in Figure 18 [151]. At low concentrations of the inorganic material, the photocurrents delivered by P3HT:aerogel electrodes are higher than those delivered by P3HT:QD films. This is related to the formation of a percolation network, required for efficient charge transport. Typically, for regular CdSe QD based solar cells, the best photovoltaic responses are obtained at high loadings of nanoparticles (~80-90 wt%), because a large amount of nanoparticles is required for the formation of a percolation network. In the case of aerogels, this effect is minimized because percolation paths are preformed during the synthesis of the gel. When the concentration of inorganic material loaded into the P3HT matrix reaches 90 wt%, the photocurrent of the QD-based electrode becomes similar to the aerogel-based electrode because at this condition both samples achieved effective formation of 3D interconnected networks. TAS data revealed that more charges are formed when using aerogels, and that these charges seem to have longer lifetime. This is possibly related to the improved screening of charges in these systems, resulting from lower recombination due to the existence of a more interconnected network. Similar experiments were performed for mixtures of P3HT:CdSe (core only) aerogels and the same trends were observed [152].

Insert Fig 18 here

Figure 18. (Left) Photocurrent responses under white light (100 mW cm^{-2}) in the presence of a 0.1 M Na_2SO_4 electrolyte saturated with O_2 and (right) transient kinetic traces (following photoexcitation at 510 nm, pump intensity ~59 mJ cm^{-2}) of films of (a) P3HT:aerogel or (b) P3HT:QDs, with (-----) 0 wt%, (—) 50 wt%, (—) 67 wt%, (—) 80 wt% and (—) 90 wt% of CdSe(ZnS). Reprinted with permission from reference [151] with permission from PCCP Owner Societies.

Similar approaches can be used to prepare thin films of connected gel networks, presenting better conductivity than a regular QD-based film [153]. This suggests that such structures could also be suitable candidates for application in all-inorganic and thin-film-based solar cells, or in hybrid devices where low amounts of inorganic phase are desired. Further investigations on the application of this synthetic approach to devices are much welcome to the field.

Ternary systems based on polymer/fullerene/QD mixtures

Ternary systems have recently attracted attention as candidates for traditional organic solar cells. Such systems can be comprised of polymer/polymer/fullerene [154,155,156,157,158,159], small organic molecule/polymer/fullerene [160,161,162], polymer/fullerene/fullerene [163,164] or polymer/inorganic nanoparticles/fullerene combinations [165,166,167,168,169]. An indicative of the growing interest in this field is the fact that at least three excellent, very enthusiastic reviews have been recently published on this subject [7·8·9]. It has been suggested that the ternary approach could be the next generation of organic solar cells, or that it could beat the Tandem architecture as a route to devices with extended light-harvesting and lower fabrication cost.

In the ternary approach, the third component is usually introduced to increase light-harvesting. Considering the incorporation of inorganic nanoparticles into the polymer/fullerene mixture, most reports use metal nanoparticles, especially Au and Ag, to take advantage of surface Plasmon resonance effects [165,166,167,168,169]. Semiconductor QDs, on the other hand, were poorly explored in these systems for quite a long time. To our knowledge, the first report of this kind of mixture was published in 2008, when Chen et al. [170] showed high photoconductive gain under low applied voltages for devices based on the incorporation of CdTe nanoparticles into a polymer/fullerene film. An external quantum efficiency as high as ~8,000 % at 350 nm was achieved at –4.5 V, attributed to the contribution of assisted hole injection into the polymer by the inorganic nanoparticles.
In 2010, De Freitas et al. [171] systematically investigated polymer/PCBM/CdSe ternary systems for application in solar cells. The polymer used was poly(9,9-n-dihexyl-2,7-fluorenilenevinylene-alt-2,5-thienylenevinylene) (PFT), which contains fluorene and thiophene units in the main chain [172]. It was found that both the concentration and size of the inorganic nanoparticles affected device performance [171,173]. At optimized conditions (~ 4.0 nm CdSe QDs and PCBM:CdSe 1:1 wt% ratio) there was an increase in Jsc and Voc, resulting in an enhancement of efficiency from 0.5 % to 0.8 % after incorporation of CdSe into the PFT/PCBM system. In this study, no ligand exchange was performed, and the use of as-synthesized TOPO-capped CdSe QDs was sufficient to improve device performance. It was suggested that CdSe QDs could contribute to light-harvesting and charge generation, but the transport of electrons and holes to the electrodes was carried out by PCBM and the polymer, respectively. Figure 19 illustrates the diagram of the energy levels, charge transfer and transport processes expected for a ternary device. The presence of QDs also changed significantly the film morphology, which also affected device performance. An example of how the film morphology changes upon incorporation of CdSe QDs and/or PCBM to a polymer film is shown in Figure 20. Moreover, the size of CdSe nanoparticles also affected Jsc, which was related to the different contributions of nanoparticles with different sizes in light absorption and in film morphology. The larger the QD, the higher was Jsc and, therefore, the efficiency [173].

Insert Fig 19 here

Figure 19. Schematic diagram of the energy levels of a ternary system solar cell showing the work function of the electrodes and the HOMO and LUMO levels of a conjugated polymer (PFT), a fullerene derivative (PCBM) and 4.0 nm-sized CdSe QDs. The arrows indicate the expected charge transfer and charge transport processes. Reprinted with permission from [171]. Copyright 2010, Royal Society of Chemistry.

Insert Fig 20 here

Figure 20. AFM images obtained in the tapping mode for P3HT films with PCBM and/or CdSe deposited onto ITO/PEDOT:PSS substrates. Reprinted with permission from [176]. Copyright 2013, Elsevier.

In the same year, Khan et al. [174] investigated devices based on the incorporation of ~ 5-6 nm CdS QDs into a P3HT:PCBM mixture (1:1:0.8 P3HT:CdS:PCBM ratio). After incorporation of CdS QDs, the PCE increased from 0.45 % to 0.87 %, due to an increase in Jsc from 2.57 mA cm^{-2} to 4.65 mA cm^{-2}. The authors attributed the performance enhancement to the formation of a charge transfer complex between P3HT and CdS, which was supported by UV–vis absorption and photoluminescence studies. Thermal annealing at 150 °C for 30 min increased Voc from 0.45 V to 0.58 V and FF from 0.32 to 0.44, resulting in a higher PCE of 0.95 %, despite a decrease observed in Jsc (2.98 mA cm^{-2}).

In 2011, Peterson et al. [175] investigated ternary systems based on P3HT/PCBM/CdSe. They used 2.5 nm CdSe QDs functionalized with the electron acceptor methyl viologen. It was observed that the addition of CdSe nanoparticles in the P3HT/PCBM mixture promoted an increase in the photocurrent in a region corresponding to the nanoparticle absorption (560–600 nm). However, for a low ratio of CdSe to PCBM, they observed that the photocurrent was accompanied by a space charge build up that limited device performance. The authors suggested that the space charge build up could be caused by deep trapping states localized either on the nanoparticle surface or at an interface of the nanoparticle with another component of the device, i.e., P3HT, LiF, PCBM or PEDOT. Alves et al. [176] showed later that the chemical structure of the polymer has a decisive influence on the efficiency of ternary systems involving QDs/polymer/fullerene. By comparing ternary systems based on polymers containing different amounts of thiophene units in the chain (PFT and P3HT), it was shown that polymers that are too coordinating towards the inorganic QDs tend to aggregate around the nanoparticles, precluding electron transport through the fullerene phase. This indicates that the polymer structure is another key factor that must carefully be taken into account in the ternary systems. The results of this work suggest that the strong interaction between S-containing 3-heylthiophene units in P3HT with CdSe QDs could be the source of the space charge build up that limited device performance in the work of Peterson et al. [175].

In 2012, Fu et al. [177] investigated hybrid solar cells based on P3HT:PCBM:CdSe mixtures in an inverted solar cell configuration with TiO_2 as electron collection layer. The incorporation of 10 wt.% of 3.5 nm CdSe QDs capped with pyridine into the P3HT:PCBM system increased the power conversion efficiency from 2.06 to 3.05 %. Jsc increased from 7.51 mA cm^{-2} to 8.15 mA cm^{-2} and Voc increased from 0.57 V to 0.60 V after the addition of CdSe. When the active film was deposited, the CdSe particles aggregated to form clusters larger than 50 nm, and it was suggested that this aggregation facilitated electron transport. The increase of Voc was attributed to an enhancement of the charge separation.

In the same year, Jotterand and Jobin [178] reported the loss of efficiency in devices after incorporation of hexadecylamine-capped CdSe QDs with diameters ranging from 2.2 nm to 6.3 nm to a P3HT:PCBM standard device. The authors expected not to use CdSe as the electron acceptor, but as an additional photo-absorber that could improve solar cell efficiency. The increase of absorbance with the addition of CdSe was indeed observed, although it did not show specific absorbance peaks at wavelength corresponding to the band gap energy of the QDs. Moreover, the maximal power generated by the photovoltaic cell was inversely proportional to the absorption. The authors attributed the loss of efficiency to the hexadecylamine coating, which acts as an insulator that traps the charges once they have been generated.

In 2013, Huang et al. [179], investigated the impact of inorganic nanoparticles (metallic and semiconductor) capped with different organic molecules in P3HT/PCBM-based devices. Six kinds of nanoparticles were investigated: gold, CdS and PbS, capped with ligands such as aromatic thiophenols or aliphatic hydrocarbonthiols. The authors reported that, regardless of the conductivity content (conducting, semiconducting, or insulating) and light absorption (transparent, visible or near-infrared absorbing), the hybrid ternary-based P3HT/PCBM device showed no sign of efficiency improvement. Among all semiconducting nanoparticles investigated, the best device was obtained with CdS capped with an aromatic thiophenol molecule, which was the only one with charge transporting aromatic surface capping agent. The efficiency of 3.91 % obtained was slightly lower than the 4.01 % of the binary P3HT/PCBM control device. Significant aggregation of CdS was observed in that work.

In the same year, oleic acid-capped CdSe tetrapods were introduced in a P3HT/$PC_{71}BM$ mixture, in concentrations of 0, 0.5, 1, 1.5, and 2 wt% [180]. The device without CdSe tetrapods delivered a Jsc of 4.78 mA cm^{-2}, a Voc of 0.51 V, a FF of 43.4 % and a PCE of 1.07 %. At 1.5 wt% CdSe concentration, the Jsc increased to 6.11 mA cm^{-2} and the PCE improved to 1.5 %. This was explained by increased light absorption, and by the elongated shape of CdSe tetrapods contributing to increase charge transport inside the active layer by collecting electrons from P3HT domains and transferring them toward the PCBM domains. The increase in Voc was related to enhanced carrier lifetime due a new interfacial energy level induced by CdSe. For larger concentrations of CdSe (□1.5 wt%), however, the Jsc rapidly decreased, which might arise due to the formation of aggregated domains of inorganic material.

A different approach was recently demonstrated by Albero et al.[181]. The authors prepared CdSe nanoparticles (3.0 nm) capped with C_{70} and observed that the chemical linkage between the nanocrystals and the fullerenes is key for an efficient charge transfer from the QD to the fullerene molecule. Three devices were investigated, with active layer composed of mixtures of P3HT with CdSe capped with C_{70} (P3HT/C_{70}–CdSe) or with CdSe capped with pyridine (P3HT/py-CdSe), and a mixture of P3HT, $PC_{70}BM$ and CdSe capped with pyridine (P3HT/$PC_{70}BM$/py-CdSe). The P3HT/py–CdSe device showed a Jsc of 2.65 mA cm^{-2}, a Voc of 0.72 V, a FF of 0.53 and a PCE of 1.01%. The P3HT/C_{70}–CdSe device showed a Jsc of 5.61 mA cm^{-2}, a Voc of 0.55 V, a FF of 0.66 and a PCE of 2.02%. The P3HT/PCBM/py–CdSe device showed a Jsc of 0.73 mA cm_{-2}, a Voc of 0.58 V, a FF of 0.27

and a PCE of 0.11%. It was observed that the introduction of C_{70} did not have a strong influence in the mean carrier lifetime under working conditions, but the modification of the polymer/QD interface with these molecules produced an important effect on the recombination dynamics by reducing its dependence with the charge density.

Other meal chalcogenide QDs have also been applied in ternary solar cells [182,183,184]. In 2010, polymer/fullerene devices embedded with small amounts of FeS_2 QDs showed a 14 % photocurrent enhancement with up to 0.3 wt% of nanoparticle loading. Jsc increased from 6.69 to 7.63 mA cm^{-2}, while Voc and FF remained nearly the same (0.66 V and 47 %, respectively). The PCE improved from 2.08 % to 2.30 %. EQE data indicated that the devices show a negligible infrared contribution from FeS_2 QDs, which have a bandgap of about 0.95 eV, and thus photocurrent improvement was attributed to enhanced charge transfer [183]. In 2013, ternary solar cells with an inverted structure were fabricated by adding TOPO-capped FeS_2 to a P3HT:PCBM active layer. The concentration of FeS_2 was varied from 0 to ~ 4 wt% and three distinct performance regimes were observed, which were correlated to microstructure transitions, as depicted in Figure 21. While the addition of FeS_2 consistently increased Jsc, the Voc and FF decreased in the devices with higher pyrite concentrations, possibly because of an increase in current leakage. By adding up to ~ 0.5 wt% of FeS_2 in the films, photocurrent enhancements of up to 20 % were consistently obtained as the FeS_2 QDs served to enhance film morphology, increasing charge generation and transport thereby. The inverted ternary hybrid solar cells demonstrate air-stability after aging 28 days exposed in air, with an actual improvement of Voc and FF that resulted in an average 28 % increase in PCE [184].

Insert Fig 21 here

Figure 21. Schematics of the microstructures of bulk heterojunction layers and possible charge transport pathways: (a) binary P3HT:PCBM layer; (b) ternary P3HT:PCBM:FeS2 layer in regime I with a low loading of FeS2, where more densely packed P3HT and PCBM domains might be formed, resulting in an enhanced charge separation at P3HT:PCBM interfaces and possibly enhanced charge transport through these domains; (c) ternary P3HT:PCBM:FeS2 layer in regime II, where an increased FeS2 loading could adversely affect device performance likely by a combination of increased leakage current, charge recombination, and/or charge trapping in defect states; (d) ternary P3HT:PCBM:FeS2 layer in regime III, where a high FeS2 loading may completely diminish Voc and FF with large leakage current and possible shorting due to nanoparticle aggregation. (e) J–V curves for all ternary devices showing three distinct performance regimes. Reprinted with permission from [184]. Copyright 2013, Elsevier.

Recently, a paper by Itskos et al. [71] brought insights on how systematic photophysical investigation of binary mixtures can be used to understand the complex behavior of ternary mixtures. The authors prepared heterojunctions of a low band-gap silicon-bridged dithiophene copolymer (Si–PCPDTBT) and oleic acid capped PbS QDs with diameters in the 2.9–9.2 nm range. Tuning the QD energy levels enabled investigations of both type II and type I polymer/QD band alignments. Pump–probe transmission was employed to study the dynamics of photogenerated species at ultrafast scales down to 200 fs. In combination with time-resolved luminescence, the two techniques provided a method to evaluate the excitation dynamics and charge-transfer processes within the films. Figure 22 shows results of steady-state and time-resolved PL of binary and ternary mixtures, and an overall picture of the electron/hole-transfer proposed for the ternary systems as a function of the QD size. The polymer/QD hybrid film containing smaller dots (2.9 nm) exhibited a highly efficient quenching of the PbS emission, indicating the formation of type II band alignment. On the other hand, a negligible emission reduction was observed from the hybrid based on the 4.3 nm-sized QD, indicative of a crossover to type I energetic alignment. It was demonstrated that the incorporation of a small fullerene fraction does not vary emission quenching significantly in the films with smaller QDs, while it improves it significantly in the film with larger QDs, as an interfacial electron-transfer channel to the fullerene component becomes available. Both ternary films show an efficient QD lifetime shortening after addition of PCBM. Curiously, the authors conclude their paper suggesting that the employment of post-fabrication ligand exchange processes, which could enable the simultaneous activation of efficient electron and hole extraction, may be a better alternative than the use of ternary systems for developing more efficient devices.

Insert Fig 22 here

Figure 22. (a,b) Steady-state and (c,d) time-resolved PL quenching data from pristine QD (blue), binary polymer–QD (orange), and ternary polymer–fullerene–QD films (green). (a,c) refer to films based on 2.9-nm-sized QDs while (b,d) were on 4.3-nm-sized QDs. Pristine and ternary decays are fitted by double exponentials (red lines) dominated by the lifetimes displayed in the graph. The inset shows the polymer and binary QD film decays recorded at the peak of the hybrid PL. Reprinted with permission from [71]. Copyright 2013, Wiley.

Ten Cate et al. [185] combined ultrafast TAS measurements with ultrafast time-resolved terahertz spectroscopy to investigate the efficiency of charge transfer and the mobility of charges in films prepared with PbS/P3HT, PbS/PCBM and PbS/P3HT/PCBM mixtures and gain better underrating of these systems. The PbS QDs used were capped with oleic acid and had an average diameter of 2.5 nm. It was found that the quantum efficiency for hole transfer to P3HT is lower than that for electron transfer to PCBM. This result was related to a limited interfacial contact between the polymer chains and the PbS QD surface that contains bulky oleic acid capping molecules. In addition, local structural disorder in the form of kinks and torsions along a P3HT chain enhances the ionization potential, which may cause the driving force for hole transfer to become energetically unfavorable. Interestingly, it was found that the quantum yields for electron and hole transfer from PbS QDs in the ternary and binary systems are comparable. Furthermore, it was found that the mobilities of electrons and holes originating from charge transfer from a photoexcited PbS QD is smaller than for direct charge generation within a P3HT:PCBM, both in the binary and in the ternary system. Furthermore, the average mobility of charges directly generated in a P3HT:PCBM domain is negatively affected by the

presence of QDs in the ternary blend. The authors suggested that charge transfer from a PbS QD in a bulk heterojunction with PCBM or P3HT leads to a charge localized within the inorganic nanoparticle and a counter charge in the organic material, which strongly reduces the charge mobility and the ability to escape from recombination. Therefore, it was concluded that the device efficiency will be limited by the coulomb interaction between the electron on a CdSe QD and the hole in P3HT, even in the absence of charge trapping in QD surface defects. In this case, one may conclude that, independent on the quality of QDs used in the ternary system, there is an intrinsic limitation to improve device efficiency.

Overall, considering ternary systems containing inorganic semiconductor nanoparticles, three particular aspects must be highlighted:

- There is a certain discrepancy between the results published by different research groups; while some authors see improvements upon incorporation of inorganic semiconductor nanoparticles as ternary components, others only see loss of device performance.
- Although some reports show improvement of photocurrent and PCE for ternary devices in comparison to binary polymer/fullerene devices, the efficiency values are not more expressive than the ones reported for classical polymer/fullerene binary devices.
- Most contributions present the same set of experimental tools to analyze the systems.

As one may notice, there is discrepancy among results from contributions of different research groups in terms of device performance. This is not unexpected, considering that even binary polymer/QD devices show a broad range of performance and heterogeneity in results obtained by different groups. This can be supported by the fact that there are too many parameters that significantly affect such systems, from the nanoparticle characteristics during synthesis, to the final film morphology. Moreover, since the ternary systems deal with a larger number of components, morphology may be even more crucial. This raises an important observation that when such systems are used in solar cells, direct comparison should only be made among systems with the same preparation conditions and assembly/testing protocols.

Furthermore, detailed and systematic analysis of ternary mixtures is still missing. Most works use the same set of traditional characterization techniques, which are not enough anymore to go to the next level of understanding of such complex systems. New data and more meaningful insights must be provided. For example, techniques such as electron tomography, used for a detailed study of film morphology in polymer/CdSe systems, have not yet been used to investigate the ternary hybrid films. Kelvin probe or conductive AFM images to map the sites where the inorganic particles are located also tools that can be helpful.

Another point of concern is that, although some works clearly show an increase of the efficiency for ternary devices compared to classical polymer/fullerene binary systems, in none of them the standard binary polymer/fullerene device used as reference had a highly efficient performance as has already been reported for polymer/fullerene solar cells. This could raise the question if such ternary systems are really advantageous and bring real improvements to device efficiency, or if it is just a matter of artefacts related to an incomplete mastering of the standard system used as reference. There is a chance that the introduction of nanoparticles only increase the efficiency in polymer/fullerene systems which are not optimized, i.e., where the morphology is not adequate. More work is necessary to clarify this point.

Despite all the issues related to ternary systems, this field is very complex and challenging, and there is much room for improvements. At least from a scientific point of view, because much insightful learning could be drawn from them and because this is an opportunity for application of knowledge from many areas of materials science, such systems do deserve attention and further investigations.

Conclusions and Perspectives

Polymer/QD solar cells have shown increasing popularity in the scientific community. Although efficiencies are around 3-4 % to date, and thus are not in the same scale as those obtained for all-inorganic solar cells based on PbS/ZnO (~ 7 %) or organic solar cells (~ 10 %), such systems are still considered very promising and the number of research groups publishing in this field is growing. An analysis of the environmental aspects of future polymer/nanoparticle solar cells through life cycle analysis was reported in 2010, indicating that these devices have potential to compete with other photovoltaic technologies[186].

A comprehensive analysis of the literature reveals discrepancy between the results published by different research groups. This is not completely unexpected, once such systems are very complex. There are many parameters that affect the device performance, including: chemical composition, size, shape and structural quality of the nanoparticles; surface ligands and the interface between the inorganic material and polymer; morphology of the resulting hybrid film; etc. Simple parameters, such as solvent employed during film deposition, and post-production treatments (with organic molecules or thermal annealing) have proved to be crucial. Because many parameters affect device performance, it becomes extremely case sensitive. As a consequence, the conversion efficiencies achieved for hybrid solar cells vary considerably amongst different research groups, even if they use similar approaches. Direct comparison of results among different research works may be tricky in this sense.

It is interesting to notice that a few years ago the route to improve efficiency seemed to be through the use of complex, branched particle geometries. The scenario has changed and lately the highest efficiencies have been obtained with spherical nanoparticles. This is good news for young research groups working in the area, considering that the synthesis of spherical

QDs is easier compared to tetrapods, for example. That does not mean, however, that synthetic procedures can be carried out without the most careful and systematic way, as the quality of the resulting material clearly affects device performance.

Sometimes, a decreased device performance is observed when chalcogenide nanoparticles are used. In these cases, very often one sees a significant decrease in the fill factor of the devices, even if they present high Voc values. This is possibly related to a current leakage, and/or recombination in the interface of inorganic nanoparticles with polymers, which has been related to trapping, probably at the QD surface or at the interface between this material and the polymer, due to many defects present at these materials or inadequade type of ligands/formation of band offset hererojunctions.

The control of the polymer/QD interface remains a challenge. While some groups are working on a complete removal of capping ligands from the QD surfaces to produce inorganic nanoparticles in a more intimate contact with the polymer, using methods such as the *in situ* synthesis of QDs in a polymer solution or polymer film, others are betting at polymer-grafting methods. These are elegant approaches, which have not led to record efficiencies yet, but they have provided important information about charge generation and recombination in the hybrid systems. It is expected that those approaches might also provide tools for reaching a next generation of efficient devices.

Considering the fabrication and prototyping of hybrid devices and a more commercial point of view, strategies related to post-production treatments (such as treatments with thiol molecules or washing procedures with acids), or procedures to adapt film formation (such as dissolving the materials separately in different solvents), are considered more straightforward alternatives for improving efficiency. It is important to mention that the current record efficiency of 4.1 % was obtained for a CdS/P3HT device by modulating the morphology through manipulation of solvents and film formation. Efforts in this direction are very welcome to the field, and the expectations are that the route to increasing device efficiency should be possible by manipulating the surface chemistry of QDs, polymer/QD interfaces and film morphology, with the use of post-production techniques.

Another concern of specialists in the field of solar energy is to encourage the development of devices prepared from materials that are earth abundant. PbS is considered to fulfil these requirements. For many years devices made from the combination of Pb-based chalcogenides with conjugated polymers presented very low efficiencies, of about 10-fold lower than those obtained with Cd-based chalcogenide nanoparticles. This drawback has been overcome in the past few years, as scientists began to combine post-production treatments with thiol-based molecules and the use of low bandgap polymers with energy levels more suitable to form a type II heterojunction with PbS or PbSe nanoparticles. Efficiencies of such devices are now reaching 2-3 %, suggesting that they can soon become competitive with devices assembled with CdS and CdSe, or even lead to more efficient hybrid solar cells, as PbS and PbSe have potential to enhance light harvesting.

To accelerate the development of the field, it is also crucial that novel techniques and tools be used, to take the understanding of hybrid systems to the next level. Techniques and combination of techniques that could provide further insights into the hybrid film nanomorphology and correlate it with charge generation and extraction are needed. This is even more crucial in the case of ternary devices, which combine inorganic nanoparticles with polymer and fullerene derivatives, since such systems have more interfaces and probably have a more complicated morphology. Although there is much controversy about the true efficacy of using ternary systems, some authors believe that they are very promising and might allow reaching enhanced light harvesting while keeping a simple device architecture.

Last, but not least, reproducibility and stability have been poorly demonstrated in hybrid systems so far. After optimization of device efficiency, the next step will require special attention for the long-term stability of these systems. This will probably bring new challenges, as it is known nanocrystals surfaces can easily suffer oxidation. The outlook of this field should also include the demonstration of stability and reproducibility of the devices, and this kind of analysis should become a part of daily routine for researchers working in the field.

Acknowledgements

The authors acknowledge FAPESP, CNPq and CAPES for financial support.

Notes and references

[a] Center of Information Technology Renato Archer - CTI, Rodovia D. Pedro I, Km 143,6, 13069-901, Campinas – SP, Brazil.
[b] Chemistry Institute, University of Campinas - UNICAMP, P.O. Box 6154, 13083-970, Campinas – SP, Brazil.
* anaflavia@iqm.unicamp.br; jilian.freitas@cti.gov.br

[1] A. J. Nozik, M. C. Beard, J. M. Luther, M. Law, R. J. Ellingson and J. C. Johnson, *Chem. Rev.*, 2010, **110**, 6873.
[2] D. Bera, L. Qian, T.-K. Tseng and P. H. Holloway, *Materials*, 2010, **3**, 2260.
[3] D. V. Talapin, J.-S. Lee, M. V. Kovalenko and E. V. Shevchenko, *Chem. Rev.*, 2010, **110**, 389.
[4] R. Debnath, O. Bakr and E. H. Sargent, *Energy Environ. Sci.*, 2011, **4**, 4870.

[5] N. Tomczak, D. Janczewski, M. Han and G. J. Vancso, *Prog. Polym. Sci.*, 2009, **34**, 393.
[6] B. R. Saunders and M. Turner, *Adv. Colloid Interface Sci.*, 2008, **138**, 1.
[7] T. Ameri, P. Khoram, J. Min and C. J. Brabec, *Adv. Mater.*, 2013, **25**, 4245.
[8] Y.-C. Chen, C.-Y. Hsu, R. Y.-Y. Lin, K.-C. Ho and J. T. Lin, *Chem. Sus. Chem.*, 2013, **6**, 20.
[9] L. Yang, L. Yan and W. You, *J. Phys. Chem. Lett.*, 2013, **4**, 1802.
[10] B. R. Saunders, *J. Colloid Interface Sci*., 2012, **369**, 1.
[11] T. Xu and Q. Qiao, *Energy Environ. Sci.*, 2011, **4**, 2700.
[12] M. Wright and A. Uddin, *Sol. Energy Mater. Sol. Cells*, 2012, **107**, 87.
[13] J. Albero, J. N. Clifford and E. Palomares, *Coord. Chem. Rev.*, 2013, **263-264**, 53.
[14] H. Wei, H. Zhang, H. Sun and B. Yang, *Nano Today*, 2012, **7**, 316.
[15] C. J. Stolle, T. B. Harvey and B. A. Korgel, *Curr. Opin. Chem. Eng*., 2013, **2**, 160.
[16] J. Chandrasekaran, D. Nithyaprakash, K. B. Ajjan, S. Maruthamuthu, D. Manoharan and S. Kumar, *Renew. Sustain. Energy Rev.*, 2011, **15**, 1228.
[17] P. Reiss, E. Couderc, J. De Girolamo and A. Pron, *Nanoscale*, 2011, **3**, 446.
[18] K. D. G. I. Jayawardena, L. J. Rozanski, C. A. Mills, M. J. Beliatis, N. A. Nismy and S. R. P. Silva, *Nanoscale*, 2013, **5**, 8411.
[19] J. Boucle and J. Ackermann, *Polym. Int.*, 2012, **61**, 355.
[20] H. K. Jun, M. A. Careem and A. K. Arof, *Renew. Sust. Energ. Rev.*, 2013, **22**, 148.
[21] P. V. Kamat, *Acc. Chem. Res.*, 2012, **45**, 1906.
[22] P. V. Kamat, K. Tvrdy, D. R. Baker and J. G. Radich, *Chem. Rev.*, 2010, **110**, 6664.
[23] L. Etgar, *Materials*, 2013, **6**, 445.
[24] N. C. Greenham, X. Peng and A. P. Alivisatos, *Phys. Rev. B: Condens. Matter*, 1996, **54**, 17628.
[25] W. U. Huynh, J. J. Dittmer and A. P. Alivisatos, *Science*, 2002, **295**, 2425.
[26] J. C. Hindson, Z. Saghi, J.-C. Hernandez-Garrido, P. A. Midgley and N. C. Greenham, *Nano Lett.*, 2011, **11**, 904.
[27] Y. Zhou, Y. C. Li, H. Z. Zhong, J. H. Hou, Y. Q. Ding, C. H. Yang and Y. F. Li, *Nanotechnology*, 2006, **17**, 4041.
[28] B. Q. Sun, E. Marx and N. C. Greenham, *Nano Lett.*, 2003, **3**, 961.
[29] I. Gur, N. A. Fromer, C.-P. Chen, A. G. Kanaras and A. P. Alivisatos, *Nano Lett.*, 2007, **7**, 409.
[30] G. Grancini, M. Biasiucci, R. Mastria, F. Scotognella, F. Tassone, D. Polli, G. Gigli and G. Lanzani, *J. Phys. Chem. Lett.*, 2012, **3**, 517.
[31] K.-S. Lee, I. Kim, S. Gullapalli, M. S. Wong and G. E. Jabbour, *Appl. Phys. Lett.*, 2011, **99**, 223515.
[32] S. Dayal, M. O. Reese, A. J. Ferguson, D. S. Ginley, G. Rumbles and N. Kopidakis, *Adv. Funct. Mater.*, 2010, **20**, 2629.
[33] B. Q. Sun, H. J. Snaith, A. S. Dhoot, S. Westenhoff and N. C. Greenham, *J. Appl. Phys.*, 2005, **97**, 014914.
[34] W. U. Huynh, J. J. Dittmer, W. C. Libby, G. L. Whiting and A. P. Alivisatos, *Adv. Funct. Mater.*, 2003, **13**,73.
[35] B. Q. Sun and N. C. Greenham, *Phys. Chem. Chem. Phys.*, 2006, **8**, 3557.
[36] L. Wang, Y. S. Liu, X. Jiang, D. H. Qin and Y. Cao, *J. Phys. Chem. C*, 2007, **111**, 9538.
[37] L. L. Han, D. H. Qin, X. Jiang, Y. S. Liu, L. Wang, J. W. Chen and Y. Cao, *Nanotechnology*, 2006, **17**, 4736.
[38] S. Dayal, N. Kopidakis, D. C. Olson, D. S. Ginley and G. Rumbles, *Nano Lett.*, 2010, **10**, 239.
[39] D. Celik, M. Krueger, C.Veit, H. F. Schleiermacher, B. Zimmermann, S. Allard, I. Dumsch, U. Scherf, F. Rauscher and P. Niyamakom, *Sol. Energy Mater. Sol. Cells*, 2012, **98**, 433.
[40] S.-H. Choi, H. J. Song, I. K. Park, J.-H. Yum, S.-S. Kim, S. H. Lee and Y.-E. Sung, *J. Photochem. Photobiol. A*, 2006, **179**, 135.
[41] A.-W. Tang, F. Teng, H. Jui, Y.-H. Gao, Y.-B. Hou, C.-J. Liang and Y.-S. Wang, *Mater. Lett.*, 2007, **61**, 2178.
[42] Y. F. Zhou, F. S. Riehle, Y. Yuan, H.-F. Schleiermacher, M. Niggemann, G. A. Urban and M. Krüger, *Appl. Phys. Lett.*, 2010, **96**, 013304.
[43] Y. Zhou, M. Eck and M. Krueger, *Energy Environ. Sci.*, 2010, **3**, 1851.
[44] Y. Zhou, M. Eck, C. Veit, B. Zimmermann, F. Rauscher, P. Niyamakom, S.Yilmaz, I. Dumsch, S. Allard, U. Scherf and M. Kruger, *Sol. Energy Mater. Sol. Cells*, 2011, **95**, 1232.
[45] Y. Zhou, M. Eck, C. Men, F. Rauscher, P. Niyamakom, S. Yilmaz, I. Dumsch, S. Allard, U. Scherf and M. Krüger, *Sol. Energy Mater. Sol. Cells*, 2011, **95**, 3227.
[46] J. Yang, A. Tang, ,R. Zhou and J. Xue, *Sol. Energy Mater. Sol. Cells*, 2011, **95**, 476.
[47] W. F. Fu, Y. Shi, W. M. Qiu, L. Wang, Y. X. Nan, M. M. Shi, H. Y. Li and H. Z. Chen, *Phys. Chem. Chem. Phys.*, 2012, **14**, 12094.
[48] W.-F. Fu, Y. Shi, L. Wang, M.-M. Shi, H.-Y Li and H.-Z. Chen, *Sol. Energy Mater. Sol. Cells*, 2013, **117**, 329.
[49] S. Ren, L.-Y. Chang, S.-K. Lim, J. Zhao, M. Smith, N. Zhao, V. Bulovic, M. Bawendi and S. Gradecak, *Nano Lett.*, 2011, **11,** 3998.
[50] S. K. Dixit, S. Madan, D. Madhwal, J. Kumar, I. Sihgh, C. S. Bhatia, P. K. Bhatnagar and P. C. Mathur, *Org. Electron.*, 2012, **13**, 710.

[51] C.-Y. Kuo, M.-S. Su, G.-Y. Chen, C.-S. Ku, H.-Y. Lee and K.-H. Wei, *Energy Environ. Sci.*, 2011, **4**, 2316.
[52] F. Qiao, *Solid-State Electron.*, 2013, **82**, 25.
[53] Y. Peng, G. Song, X. Hu, G. He, Z. Chen, X. Xu and J. Hu, *Nanoscale Res. Lett.*, 2013, **8**, 106.
[54] R. Zhou, Y. Zheng, L. Qian, Y. Yang and P. H. Holloway, J. Xue, *Nanoscale*, 2012, **4**, 3507.
[55] Y. Wu and G. Zhang, *Nano Lett.*, 2010, **10**, 1628.
[56] T. Vossmeyer, L. Katsikas, M. Giersig, I. G. Popovic, K. Diesner, A. Chemseddine, A. Eychmuller, and H. Weller, *J. Phys. Chem.*, 1994, **98**, 7665.
[57] I. Moreels, K. Lambert, D. Smeets, D.D. Muynck, T. Nollet, J.C. Martins, F. Vanhaecke, A. Vantomme, C. Delerue, G. Allan and Z. Hens, *ACS Nano*, 2009, **3**, 3023.
[58] O.E. Semonin, J.M. Luther, S. Choi, H.-Y. Chen, J. Gao, A.J. Nozik and M.C. Beard, *Science*, 2011, **334**, 1530.
[59] A. A. R. Watt, D. Blake, J. H. Warner, E. A. Thomsen, E. L. Tavenner, H. Rubinsztein-Dunlop and P. Meredith, *J. Phys. D Appl. Phys.*, 2005, **38**, 2006.
[60] S. A. McDonald, G. Konstantatos, S. G. Zhang, P. W. Cyr, E. J. D. Klem, L. Levina and E. H. Sargent, *Nat. Mater.*, 2005, **4**, 138.
[61] A. Maria, P.W. Cyr, E.J.D. Klern, L. Levina and E.H. Sargent, *Appl. Phys. Lett.*, 2005, **87**, 213112.
[62] D. Cui , J. Xu , T. Zhu , G. Paradee , S. Ashok and M. Gerhold, *Appl. Phys. Lett.*, 2006, **88**, 138111 .
[63] X. M. Jiang, R. D. Schaller, S. B. Lee, J. M. Pietryga, V. I. Klimov and A. A. Zakhidov, *J. Mater. Res.*, 2007, **22,** 2204.
[64] S. Günes, K. P. Fritz, H. Neugebauer, N. S. Sariciftci, S. Kumar and G. D. Scholes, *Sol. Energy Mater. Sol. Cells*, 2007, **91**, 420 .
[65] K. P. Fritz, S. Guenes, J. Luther, S. Kumar, N. S. Sacriciftci and G. D. Scholes, *J. Photochem. Photobiol.* A, 2008, **195**, 39.
[66] Z. Wang, S. Qu, X. Zeng, C. Zhang, M. Shi, F. Tan, Z. Wang, J. Liu, Y. Hou, F. Teng and Z. Feng, *Polymer*, 2008, **49**, 4647.
[67] Z. Tan, T. Zhu, M. Thein, S. Gao, A. Cheng, F. Zhang, C. Zhang, H. Su, J. Wang, R. Henderson, J.-I. Hahm, Y. Yang and J. Xu, *Appl. Phys. Lett.*, 2009, **95**, 063510 .
[68] D. Yun, W. Feng, H. Wu and K. Yoshino, *Sol. Energy Mater. Sol. Cells*, 2009, **93**, 1208.
[69] Seo, J.; Kim, S. J.; Kim, W. J.; Singh, R.; Samoc, M.; Cartwright, A. N.; Prasad, P. N. *Nanotechnology*, 2009, **20**, 095202.
[70] K. M. Noone, N. C. Anderson, N. E. Horwitz, A. M. Munro, A. P. Kulkarni and D. S. Ginger, *ACS Nano*, 2009, **3**, 1345.
[71] G. Itskos, P. Papagiorgis, D. Tsokkou, A. Othonos, F. Hermerschmidt, S. P. Economopoulos, M. Yarema, W. Heiss, S. Choulis, *Adv. Energy Mater.*, 2013, **3**, 1490.
[72] K. M. Noone, E. Strein, N. C. Anderson, P.-T. Wu, S. A. Jenekhe, D. S. Ginger, *Nano Lett.*, 2010, **10**, 2635.
[73] J. Seo, M. J. Cho, D. Lee, A. N. Catwright and P. N. Prasad, *Adv. Mater.*, 2011, **23**, 3984.
[74] Y. Zhang, Z. Li, J. Ouyang, S.-W. Tsang, J. Lu, K. Yu, J. Ding and Y. Tao, *Org. Electron.*, 2012, **13**, 2773.
[75] C. Piliego, M. Manca, R. Kroon, M. Yarema, K. Szendrei, M. R. Andersson, W. Heiss and M. A. Loi, *J. Mater. Chem.*, 2012, **22**, 24411.
[76] M. Nam, S. Kim, S. Kim, S.-W. Kim and K. Lee, *Nanoscale*, 2013, **5**, 8202.
[77] A. E. Colbert, E. M. anke, S. T. Hsieh, S. Subramaniyan, C. W. Schlenker, S. A. Jenekhe and D. S. Ginger, *J. Phys. Chem. Lett.*, 2013, **4**, 280.
[78] J. Tang, K. W. Kemp, S. Hoogland, K. S. Jeong, H. Liu, L. Levina, M. Furukawa, X. Wang, R. Debnath, D. Cha, K. W. Chou, A. Fischer, A. Amassian, J. B. Asbury and E. H. Sargent, *Nat. Mater.*, 2011, **10**, 765.
[79] A. H. Ip, S. M. Thon, S. Hoogland, O. Voznyy, D. Zhitomirsky, R. Debnath, L. Levina, L. R. Rollny, G. H. Carey, A. Fischer, K. W. Kemp, I. J. Kramer, Z. Ning, A. J. Labelle, K. W. Chou, A. Amassian, and E. H. Sargent, *Nat. Nanotechnology*, 2012, **7**, 577.
[80] Z. Wang, S. Qu, X. Zeng, J. Liu, C. Zhang, F. Tan, L. Jin, and Z. Wang, *J. Alloy. Compd.*, 2009, **482**, 203.
[81] Y-Y. Lin, D.-Y. Wang, H.-C. Yen, H.-L. Chen, C.-C. Chen, C.-M. Chen, C.-Y. Tang and C.-W. Chen, *Nanotechnology*, 2009, **20**, 405207.
[82] C. Steinhagen, T. B. Harvey, C. J. Stolle, J. Harris and B. A. Korgel, *J. Phys. Chem. Lett.*, 2012, **3**, 2352.
[83] A. Layek, S. Middya and P. P. Ray, *J. Mater. Sci.*, 2013, **24**, 3749.
[84] N. Bansal, F. T. F. O'Mahony, T. Lutz and S. A. Haque, *Adv. Energy Mater.*, 2013, **3**, 986.
[85] F. T. F. O'Mahony, U. B. Cappel, N. Tokmoldin, T. Lutz, R. Lindblad and H. Rensmo, *Ang. Chem. Int. Ed.*, 2013, **52**, 12047.
[86] C. Wadia, A. P. Alivisatos and D. M. Kammen, *Environ. Sci. Technol.,* 2009, **43**, 2072.
[87] A. Ennaoui, S. Fiechter, C. Pettenkofer, N. Alonsovante, K. Buker, M. Bronold, C. Hopfner and H. Tributsch, *Sol. Energy Mater. Sol. Cells*, 1993, **29**, 289.
[88] E. Arici, N. S. Sariciftci and D. Meissner, Adv. Funct. Mater., 2003, 13, 165.

[89] W. Yue, S. Han, R. Peng, W. Shen, H. Geng, F. Wu, S. Tao and M. Wang, *J. Mater. Chem.*, 2010, **20**, 7570.

[90] E. Maier, T. Rath, W. Haas, O. Werzer, R. Saf, F. Hofer, D. Meissner, O. Volobujeva, S. Bereznev, E. Mellikov,
H. Amenitsch, R. Resel and G. Trimmel, *Sol. Energy Mater. Sol. Cells*, 2011, **95**, 1354.

[91] T. Rath, M. Edler, W. Haas, A. Fischereder, S. Moscher, A. Schenk, R. Trattnig, M. Sezen, G. Mauthner, A. Pein, D. Meischler, K. Bartl, R. Saf, N. Bansal, S. A. Haque, F. Hofer, E. J. W. List, G. Trimmel, *Adv. Energy Mater.*, 2011, **1**, 1046.

[92] N. Radychev, D. Scheunemann, M. Kruszynska, K. Frevert, R. Miranti, J. Kolny-Olesiak, H. Borchert and J. Parisi, *Org. Electron.*, 2012, **13**, 3154.

[93] M. Arar, M. Gruber, M. Edler, W. Haas, F. Hofer, N. Bansal, L. X. Reynolds, S. A. Haque, K. Zojer, G. Trimmel and T. Rath, *Nanotechnology*, 2013, **24**, 484005.

[94] M. Arar, A. Pein, W. Haas, F. Hofer, K. Norrman, F. C. Krebs, T. Rath and G. Trimmel, *J. Phys. Chem. C*, 2012, **116**, 19191.

[95] Y. Yang, H. Zhong, Z. Bai, B. Zou, Y. Li and G. D. Scholes, *J. Phys. Chem. C*, 2012, **116**, 7280.

[96] J. Kolny-Olesiak and H. Weller, *ACS Appl. Mater. Interfaces*, 2013, **5**, 12221.

[97] D. Aldakov, A. Lefrançois and P. Reiss, *J. Mater. Chem. C*, 2013, **1**, 3756.

[98] J. E. Brandenburg, X. Jin, M. Kruszynska, J. Ohland, J. Kolny-Olesiak, I. Riedel, H. Borchert and J. Parisi, *J. Appl. Phys.*, 2011, **110**, 064509.

[99] A. Hassinen, I. Moreels, K. D. Nolf, P. F. Smet, J. C. Martins and Z. Hens, *J. Am. Chem. Soc.*, 2012, **134**, 20705.

[100] M. A. Green, K. Emery, Y. Hishikawa, W. Warta, E. D. Dunlop, *Prog. Photovolt. Res.*, 2012, **20**, 12.

[101] Z. Li, F. Gao, N. C. Greenham and C. R. McNeill, *Adv. Funct. Mater.*, 2011, **21**, 1419.

[102] K.M. Noone, S. Subramaniyan, Q. Zhang, G. Cao, S.A. Jenekhe and D.S. Ginger, *J. Phys. Chem. C.*, 2011, **115**, 24403.

[103] M. D. Heinemann, K. von Maydell, F. Zutz, J. Kolny-Olesiak, H.
Borchert, I. Riedel and J. Parisi, *Adv. Funct. Mater.*, 2009, **19**, 3788.

[104] S. H. Choi, S. H. Lee and Y. E. Sung, *Appl. Chem.*, 2003, **7**, 85.

[105] N. T. N. Truong, W. K. Kim and C. Park, *Sol. Energy Mater. Sol. Cells*, 2011, **95**, 167.

[106] J. S. Liu, T. Tanaka, K. Sivula, A. P. Alivisatos and J. M. J. Fréchet, *J. Am. Chem. Soc.*, 2004, **126**, 6550.

[107] N. C. Greenham, X. G. Peng and A. P. Alivisatos, *Phys. Rev. B*, 1996, **54**, 17628.

[108] J. Albero, E. Martınez-Ferrero, J. Ajuria, C. Waldauf, R. Paciosc and E. Palomares, *Phys. Chem. Chem. Phys.*, 2009, **11**, 9644.

[109] J. Liu, T. Tanaka, K. Sivula, A. P. Alivisatos and J. M. J. Frechet, *J. Am. Chem. Soc.*, 2004, **126**, 6550.

[110] R. Rhodes, P. Obrien and B.R. Saunders, *J. Colloid Interface Sci.*, 2011, **358**, 151.

[111] S. A. Dowland, L. X. Reynolds, A. McLachlan, U. B. Cappel and S. A. Haque, *J. Mater. Chem. A*, 2013, **1**, 13896.

[112] U. B. Cappel, S. A. Dowland, L. X. Reynolds, S. Dimitrov and S. A. Haque, *J. Phys. Chem. Lett.*, 2013, **4**, 4253.

[113] Y. Yin and A. P. Alivisatos, *Nature*, 2005, **437**, 664.

[114] A. J. Moulé, L. Chang, C. Thambidurai, R. Vidu and P. Stroeve, *J. Mater. Chem.*, 2012, **22**, 2351.

[115] Y. Park and R. C. Advincula, *Chem. Mater.*, 2011, **23**, 4273.

[116] D. R. Baker and P. V. Kamat, *Langmuir*, 2010, **13**, 11272.

[117] E. Talforn, E. Moysidou, R. D. Abellon, T. J. Savenije, A. Goossens, A. J. Houtepen and L. D. A. Siebbeles, *J. Phys. Chem. C*, 2010, **114**, 3441.

[118] D. S. Ginger and N. C. Greenham, *Synth. Met.*, 1999, **101**, 425.

[119] N. T. N. Truong, W. K. Kim, U. Farva, X. D. Luo and C. Park, *Sol. Energy Mater. Sol. Cells*, 2011, **95**, 3009.

[120] I. Lokteva, N. Radychev, F. Witt, H. Borchert, J. Parisi and J. Kolny-Olesiak, *J. Phys. Chem. C*, 2010, **114**, 12784.

[121] J. D. Olson, G. P. Gray and S. A. Carter, *Sol. Energy Mater. Sol. Cells*, 2009, **93**, 519.

[122] S. O. Oluwafemi and N. Revaprasadu, *Physica B*, 2009, **404**, 1204.

[123] N. Radychev, I. Lokteva, F. Witt, J. Kolny-Olesiak, H. Borchert and J. R. Parisi, *J. Phys. Chem. C*, 2011, **115**, 14111.

[124] D. J. Milliron, A. P. Alivisatos, C. Pitois, C.; Edder and J. M. J. Fréchet, *Adv. Mater.*, 2003, **15**, 58.

[125] B. C. Sih and M. Wolf, *J. Phys. Chem. C*, 2007, **111**, 17184.

[126] M. J. Greaney, S. Das, D. H. Webber, S. E. Bradforth and R. L. Brutchey, *ACS Nano*, 2012, **6**, 4222.

[127] J. Albero, E. Martınez-Ferrero, D. Iacopino, A. Vidal-Ferranac and E. Palomar, *Phys. Chem. Chem. Phys.*, 2010, **12**, 13047.

[128] B. A. MacLeod, N. E. Horwitz, E. L. Tatcliff, J. L. Jenkins, N. R. Armstrong, A. J. Giordano, P. J. Hotchkiss, S. R. Marder, C. T. Campbell and D. S. Ginger, *J. Phys. Chem. Lett.*, 2012, **3**, 1202.

[129] M. Glioboff, H. Li, K.M. Knesting, A.J. Giordano, D. Nordlund, G.T. Seidler, J.L. Bredas, S.R. Marder and D.S. Ginger, *J. Phys. Chem. C*, 2013, **117**, 15139.

[130] J. Gantz, D. Placencia, A. Giordano, S.R. Marder and N.R. Armstrong, *J. Phys. Chem. C*, 2013, **117**, 1205.

[131] J. Seo, W. J. Kim, S. J. Kim, K.-S. Lee, A. N. Cartwright, P. N. Prasad, *Appl. Phys. Lett.*, 2009, **94**, 133302.
[132] H. Zhong, Y. Zhou, Y, Yang, C. Yang and Y. Li, *J. Phys. Chem. C*, 2007, **111**, 6538.
[133] J. Bang, J. Park, J. H. Lee, N. Won, J. Nam, J. Lim, B. Y. Chang, H. J. Lee, B. Chon, J. Shin, J. B. Park, J. H. Choi, K. Cho, S. M. Park, T. Joo and S. Kim, *Chem. Mater.*, 2010, **22**, 233.
[134] Z. Xu, C. R. Hine, M. M. Maye, Q. Meng and M. Cotlet, *ACS Nano*, 2012, **6**, 4984.
[135] M. V. Kovalenko, M. I. Bodnarchuk, J. Zaumseil, J.-S. Lee and D. V. Talapin, *J. Am. Chem. Soc.*, 2010, **132**, 10085.
[136] Y. Q. Zhang and X. A. Cao, *Nanotechnology*, 2012, **23**, 275702.
[137] A. H. Ip, S. M. Thon, S. Hoogland, O. Voznyy, D. Zhitomirsky, R. Debnath, L. Levina, L. R. Rollny, G. H. Carey, A. Fischer, K. W. Kemp, I. J. Kramer, Z. Ning, A. J. Labelle, K. W. Chou, A. Amassian and E. H. Sargent, *Nat. Nanotechnology*, 2012, **7**, 577.
[138] A. A. R. Watt, P. Meredith, J. D. Riches, S. Atkinson, H. Rubinsztein-Dunlop, *Curr. Appl. Phys.*, 2004, **4**, 320.
[139] A. Watt, E. Thomsen, P. Meredith and H. Rubinsztein-Dunlop, *Chem. Commun.*, 2004, 2334.
[140] J.H. Warner, A.A.R. Watt and R.D. Tilley, *Nanotechnology*, 2005, **16**, 2381.
[141] A. Stavrinadis, R. Beal, J. M. Smith, H. E. Assender and A. A. R. Watt, *Adv. Mater.*, 2008, **20**, 3105.
[142] H. C. Liao, S. Y. Chen, and D. M. Liu, *Macromolecules*, 2009, **42**, 6558.
[143] S. Dayal, N. Kopidakis, D. C. Olson, D. S. Ginley and G. Rumbles, *J. Am. Chem. Soc.*, 2009, **131**, 17726.
[144] M. T. Khan, A; Kaur, S. K. Dhawan and S. Chand, *J. Appl. Phys.*, 2011, **110**, 044509.
[145] H. C. Leventis, S. P. King, A. Sudlow, M. S. Hill, K. C. Molloy and S. A. Haque, *Nano Lett.*, 2010, **10**, 1253.
[146] S. Dowland, T. Lutz, A. Ward, S. P. King, A. Sudlow, M. S. Hill, K. C. Molloy and S. A. Haque, *Adv. Mater.*, 2011, **23**, 2739.
[147] L. X. Reynolds, T. Lutz, S. Dowland, A. MacLachlan, S. King and S. A. Haque, *Nanoscale*, 2012, **4**, 1561.
[148] F. Todescato, A. S. R. Chesman, A. Martucci, R. Signorini and J. J. Jasieniak, *Chem. Mater.*, 2012, **24**, 2117.
[149] J. L. Mohanan, I. U. Arachchige and S. L. Brock, *Science*, 2005, **307**, 397.
[150] I. U. Arachchige and S. L. Brock, *Acc. Chem. Res.*, 2007, **40**, 801.
[151] J. N. De Freitas, L. Korala, L. X. Reynolds, S. A. Haque, S. L. Brock and A. F. Nogueira, *Phys. Chem. Chem. Phys.*, 2012, **14**, 15180.
[152] J. N. de Freitas, J. P. C. Alves, L. Korala, S. L. Brock and A. F. Nogueira, *Procedings of SPIE*, 2012, **8477**, 847711.
[153] L. Korala, L. Li and S. L. Brock, *Chem. Commun.*, 2012, **48**, 8523.
[154] M. Koppe, H. J. Egelhaaf, G. Dennler, M. C. Scharber, C. J. Brabec, P. Schilinsky and C. N. Hoth, *Adv. Funct. Mater.*, 2010, **20**, 338.
[155] F. Machui, S. Rathgeber, N. Li, T. Ameri and C. J. Brabec, *J. Mater. Chem.*, 2012, **22**, 15570.
[156] T. Ameri, J. Min, N. Li, F. Machui, D. Baran, M. Forster, K. J. Schottler, D. Dolfen, U. Scherf and C. J. Brabec, Adv. *Energy Mater.*, 2012, **10**, 1198.
[157] H. Loslein, T. Ameri, G. J. Matt, M. Koppe, H. J. Egelhaaf, A. Troeger, V. Sgobba, D. M. Guldi and C. J. Brabec, *Macromol. Commun.*, 2013, **34**, 1090.
[158] T. Ameri, T. Heumuller, J. Min, N. Li, G. Matt, U. Scherf and C. J. Brabec, *Energy Environ. Sci.*, 2013, **6**, 1796.
[159] Q. S. An, F. J. Zhang, J. Zhang, W. H. Tang, Z. X. Wang, L. L. Li, Z. Xu, F. Teng and Y. S. Wang, *Sol. Energy Sol. Cells*, 2013, **118**, 30.
[160] J. Min, T. Ameri, R. Gresser, M. Lorenz-Rothe, D. Baran, A. Troeger, V. Sgobba, K. Leo, M. Riede, D. M. Guldi and C. J. Brabec, *ACS Appl. Mat. Interfac.*, 2013, **5**, 5609.
[161] D. M. Lyons, J. Kesters, W. Maes, C. W. Bielawski and J. L. Sessler, *Synth. Met.*, 2013, **178**, 56.
[162] H. Derouiche and A. B. Mohamed, *Sci. World J.*, 2013, 914981.
[163] R. A. Street, D. Davies, P. P. Khlyabich, B. Burkhart and B. C. Thompson, *J. Am. Chem. Soc.*, 2013, **135**, 986.
[164] H. Li, Z. G. Zhang, Y. F. Li, J. Z. Wang, *Appl. Phys. Lett.*, 2012, **101**, 163302.
[165] D. H. Wang, D. Y. Kim, K. W. Choi, J. H. Seo, S. H. Im, J. H. Park, O. O. Par and A. J. Heeger, *Ang. Chem. Int. Ed.*, 2011, **50**, 5519.
[166] D. H. Wang, K. H. Park, J. H. Seo, J. Seifter, J. H. Jeon, J. K. Kim, J. H. Park, O. O. Park and A. J. Heeger, Adv. Energy Mater., 2011, **1**, 766.
[167] C. H. Kim, S. H. Cha, S. C. Kim, M. Song, J. Lee, W. S. Shin, S. J. Moon, J. H. Bahng, N. A. Kotov and S. H. Jin, *ACS Nano*, 2011, **5**, 3319.
[168] G. D. Spyropoulos, M. M. Stylianakis, E. Stratakis and E. Kymakis, *Appl. Phys. Lett.*, 2012, **11**, 213904.
[169] X. Y. Xu, A. K. K. Kyaw, B. Peng, D. W. Zhao, T. K. S. Wong, Q. H. Xiong, X. W. Sun and A. J. Heeger, *Org. Electron.*, 2013, **14**, 2360.
[170] H.-Y. Chen, M. K. F. Lo, G. Yang, H. G. Monbouquette, Y. Yang, *Nat. Nanotechnol.*, 2008, **3**, 543.
[171] J. N. de Freitas, I. R. Grova, L. C. Akcelrud, E. Arici, N. S. Sariciftci and A. F. Nogueira, *J. Mater. Chem.*, 2010, **20**, 4845.

[172] J. N. de Freitas, A. Pivrikas, B. F. Nowacki, L. C. Akcelrud, N. S. Sariciftci, A. F. Nogueira, *Synth. Met.*, 2010, **160**, 1654.
[173] J. N. de Freitas and A. F. Nogueira, *Proceedings of SPIE*, 2010, **7772**, 77721K.
[174] M. T. Khan, R. Bhargav, A. Kaur, S. K. Dhawana and S. Chand, *Thin Solid Films*, 2010, **519**, 1007.
[175] E. D. Peterson, G. M. Smith, M. Fu, R. D. Adams, R. C. Coffin and D. L. Carroll, *Appl. Phys. Lett.*, 2011, **99**, 073304.
[176] J. P. C. Alves, J. N. de Freitas, T. D. Z. Atvars and A. F. Nogueira, *Synth. Met.*, 2013, **164**, 69.
[177] H. Fu, M. Choi, W. Luan, Y.-S. Kim and S.-T. Tu, *Solid-State Electron.*, 2012, **69**, 50.
[178] S. A. Jotterand and M. Jobin, *Energy Procedia*, 2012, **31**, 117.
[179] Y.-J. Huang, W.-C. Lo, S.-W. Liu, C.-H. Cheng, C.-T. Chen and J.-K. Wang, *Sol. Energy Mater. Sol. Cells*, 2013, **116**, 153.
[180] R. Ahmad, V. Arora, R. Srivastava, S. Sapra and M. N. Kamalasanan, Phys. *Status Solidi A*, 2013, **210**, 785.
[181] J. Albero, P. Riente, J. N. Clifford, M. A. Pericàs, E. Palomares, *J. Phys. Chem. C*, 2013, **117**, 13374.
[182] S. Pichler, T. Rauch, R. Seyrkammer, M. Böberl, S. F. Tedde, J. Fürst, M. V. Kovalenko, U. Lemmer, O. Hayden and W. Heiss, *Appl. Phys. Lett.*, 2011, **98**, 053304.
[183] C. W. Lin, D. Y. Wang, Y. T. Wang, C. C. Chen, Y. J. Yang and Y. F. Chen, *Sol. Energy Mater. Sol. Cells*, 2011, **95**, 1107.
[184] B. J. Richardson, L. Zhu and Q. Yu, *Sol. Energy Mater. Sol. Cells*, 2013, **116**, 252.
[185] S. Ten Cate, J. M. Schins and L. D. A. Siebbeles, *ACS Nano*, 2012, **6**,8983.
[186] B. Azzopardi and J. Mutale, *Renew. Sustain. Energy Rev.*, 2010, **14**, 1130.

FIGURE CAPTIONS

Figure 1. Luminescence emission from CdSe(ZnS) quantum dots solutions: the size of the nanoparticles increases from ~ 2 nm to ~ 6 nm (left to the right). The emission spans across the visible part of the electromagnetic spectrum from the blue (2 nm nanocrystals) to the red (6 nm nanocrystals). Reprinted with permission from reference [5]. Copyright 2009, Elsevier.

Figure 2. Structural depictions and approximate dimensions of nanomaterials used in polymer and hybrid organic-inorganic photovoltaic cells, such as chalcogenide nanoparticles. The size ranges shown are estimates based on literature reports for these materials and carbon-based nanomaterials usually employed in "classical" organic solar cells (PCBM, $PC_{71}BM$ and SWNT). Reprinted with permission from reference [6]. Copyright 2008, Elsevier.

Figure 3. EQE of hybrid devices assembled with CdSe 7-nm-diameter nanorods with lengths 7, 30, and 60 nm, combined with P3HT. The intensity is 0.084 mW cm^{-2} at 515 nm. Reprinted with permission from [25]. Copyright 2002, The American Association for the Advancement of *Science.*

Figure 4. Images of the binarized tomographic data. The purple regions are the CdSe particles while the polymer regions are transparent. Low-density regions are shown for (a) 6:1, (b) 3:1, and (c) 2:1 nanodot-polymer blends by weight. (d) Typical aggregated region in a 6:1 nanodot-polymer blend. (e) Nanorod-polymer blend. Reprinted with permission from [26]. Copyright 2002, American Chemical Society.

Figure 5. (a) Schematic energy level diagram of P3HT, PCPDTBT, and CdSe QDs (spherical particles with a diameter of ~4.7 nm), and the chemical structure of the polymers. (b) EQE spectra of the P3HT:CdSe and the PCPDTBT:CdSe hybrid solar cells. In this particular case, CdSe nanoparticles are in the spherical form. Reprinted with permission from reference [44]. Copyright 2011, Elsevier.

Figure 6. TEM images of P3HT/CdS hybrid films synthesized (a) without grafting and (b) using grafting process by solvent exchange. The inset images show schematic representations of each; the nongrafting and grafting method is used to control the interface between CdS QDs (yellow spheres) and P3HT NWs (purple lines). (c) Optical properties of P3HT/CdS hybrid thin films with 80 wt % CdS; absorbance of the grafting sample and PL spectra of the nongrafted and grafted films. The vibronic absorption feature at 605 nm in the grafted film is clearly resolved, indicating that the crystalline P3HT NWs are preserved after CdS QDs grafting. The PL spectral intensities of the P3HT/CdS grafted hybrid films are significantly quenched, presumably due to the efficient nonradiative channel for charge transfer from P3HT to CdS phase. (d) Current-voltage (J-V) characteristics of P3HT/CdS hybrid solar cells from nongrafting, grafting and the subsequent ligand exchange. Reprinted with permission from [49]. Copyright 2011, American Chemical Society.

Figure 7. (Right) SEM micrographs for the bilayer P3HT/ CdSe(ZnS) QDs films (a) before and (b) after annealing. (Left) J–V characteristics for the solar cells fabricated using annealed bilayer P3HT/CdSe(ZnS) QD technique for different annealing times. Reprinted with permission from [50]. Copyright 2012, Elsevier.

Figure 8. (a) Energy band diagram displaying HOMO and LUMO of possible polymer donor materials, as well as valence and conduction band edge of multiple inorganic acceptors. For the inorganic materials, solid lines represent bulk energy values, whilst dotted lines represent spherical nanoparticles exhibiting quantum confinement (PbS ~2.7 nm and CdS ~4.0 nm). For P3HT and PCPDTBT, energy values reported in two different works are displayed. All energy levels were taken from literature and summarized in the review article by Wright and Uddin[] **Error! Bookmark not defined.**]. Energy structure of isolated donor and acceptor materials, showing two major types of heterojunction structures: (b) Type

I: Nested band alignment, (c) Type II: Staggered band alignment. Adapted and reprinted with permission from [12]. Copyright 2012, Elsevier.

Figure 9. (a) EQE spectra of solar cells fabricated with a planar junction configuration in an inverted device structure (ITO/ZnO/PbS/polymer/MoOx/Ag), using PbS QDs (NQD1) without polymer, and with a layer of PCPDTTBTT or PCDTBT, which originates a type II and a type I heterojunction with PbS, respectively. (b) J–V characteristics of devices under irradiation of 100 mW cm^{-2}. Reprinted with permission from [74]. Copyright 2012, Elsevier.

Figure 10. (a) External quantum efficiency (EQE) and (b) current–voltage characteristics under 100 mW cm^{-2} illumination for P3HT/PCBM (squares), P3HT/CdSe (circles), and P3HT/F8TBT (poly((9,9-dioctylfluorene)-2,7-diyl-alt-[4,7-bis(3-hexylthien-5-yl)-2,1,3-benzothiadiazole]-2,2-diyl)) (triangles) devices. Reprinted with permission from reference [101]. Copyright 2011, Willey-VCH Verlag GmbH & Co.

Figure 11. TEM images of composites consisting of CdSe (20 wt %)/P3HT-Br (top left), CdSe (20 wt %)/P3HT-NH_2 (top right), CdSe (40 wt %)/P3HT-Br (bottom left), and CdSe (40 wt %)/P3HT-NH_2 (bottom right), respectively. The functional end-group in P3HT-NH_2 reduces the aggregation of CdSe nanorods in the composites. Reprinted with permission from reference [109]. Copyright 2004, American Chemical Society.

Figure 12. (Left) Cyclic Voltammetry measurements that allow the calculations for the reduction onset values of CdSe(non-ligand exchanged, NL) (1), CdSe(pyridine, Py) (2), and CdSe(tert-butylthiol, tBT) (3): 0.57, 0.50, and 0.66 V, respectively. (Right) Current-voltage curves for devices assembled with ITO/PEDOT:PSS/P3HT:CdSe/Al structure, made with CdSe(NL) (1), CdSe(Py) (2), or CdSe(tBT) (3) nanoparticle acceptors. Reprinted with permission from reference [126].Copyright 2012, American Chemical Society.

Figure 13. (Top) Aromatic thiol derivates used to coat the surface of CdSe QDs. The arrows indicate the direction of the dipole at the molecule. The calculated dipole moment is also shown for each molecule. (Bottom) Transient absorption decay measurements for the different films at room temperature (λ_{ex} = 470 nm and λ_{probe} = 980 nm). Reprinted with permission from reference [127] with permission from PCCP Owner Societies.

Figure 14. (Left) Scheme of the synthesis of P3HT/CdS composites by *in situ* synthesis of CdS spherical nanocrystals or nanorods via reaction of cadmium acetate dehydrate and sulfur in the presence of the polymer, dimethylsulfoxide and dichlorobenzene. The Cd^{2+} ions are assumed to be coupled with the unpaired S along the P3HT planar chain network. (Right) Average aspect ratio of CdS nanocrystals plotted as a function of the reaction time for the CdS nanorods growth. Reprinted with permission from [142]. Copyright 2009, American Chemical Society.

Figure 15. (a) Devices architectures and (b) current-voltage characteristics of CdS/P3HT solar cells. Devices (i), (ii), and (iii) employed CdS/P3HT films that were annealed at 105, 120, and 160 °C, respectively. Devices (i)–(iii) were fabricated using device Architecture A. Device (iv) was fabricated using Architecture B and employed a CdS/P3HT photoactive layer that was annealed at 160 ° C. Reprinted with permission from reference [146]. Copyright 2011, Willey-VCH Verlag GmbH & Co.

Figure 16. (Top) TEM images of equivalently loaded P3HT/CdS misxtures: a) oleic-capped CdS QDs, b) hexylamine-capped CdS QDs, c) *in situ* grown CdS. Darker regions are the inorganic component. Scale bars are 50 nm. (Bottom) Transient absorption decays for films of pristine P3HT (black), P3HT/CdS QDs with oleic acid (red) or hexylamine (green) capping ligands, and two P3HT/*in situ* grown CdS films of different ratios (blue and magenta). Excitation was set at 550 nm and 60 mJ cm^{-2} and the absorption was probed at 980 nm. Inset: transient absorption spectrum at 10 ms for a P3HT/*in situ* grown CdS film (blue)

and for a P3HT/hexylamine QD film (green) showing a ground state bleach and the $P3HT^{+}$ polaron peak. Reprinted with permission from reference [147]. Copyright 212, Royal Society of Chemistry.

Figure 17. Scheme and associated TEM micrographs showing the gel formation, via a viscous sol, of metal chalcogenide nanoparticles that are surface-capped with thiolates (RS-). Upon introduction of an oxidant, disulfides are formed (RS–SR), providing open sites on the particle surface for assembly into oligomers and eventually polymers (gels). Representative thiols (RS–H) and oxidants are also illustrated. The micrographs are of CdSe materials [prepared with ca. 3 nm spherical particles using MUA for capping and tetranitromethane (TNM) for oxidation, with the bar corresponding to 100, 20, and 20 nm, respectively, from left to right. Reprinted with permission from reference [150]. Copyright 2007, American Chemical Society.

Figure 18. (Left) Photocurrent responses under white light (100 mW cm^{-2}) in the presence of a 0.1 M Na_2SO_4 electrolyte saturated with O_2 and (right) transient kinetic traces (following photoexcitation at 510 nm, pump intensity ~59 mJ cm^{-2}) of films of (a) P3HT:aerogel or (b) P3HT:QDs, with (-----) 0 wt%, (▬) 50 wt%, (▬) 67 wt%, (▬) 80 wt% and (▬) 90 wt% of CdSe(ZnS). Reprinted with permission from reference [151] with permission from PCCP Owner Societies.

Figure 19. Schematic diagram of the energy levels of a ternary system solar cell showing the work function of the electrodes and the HOMO and LUMO levels of a conjugated polymer (PFT), a fullerene derivative (PCBM) and 4.0 nm-sized CdSe QDs. The arrows indicate the expected charge transfer and charge transport processes. Reprinted with permission from [171]. Copyright 2010, Royal Society of Chemistry.

Figure 20. AFM images obtained in the tapping mode for P3HT films with PCBM and/or CdSe deposited onto ITO/PEDOT:PSS substrates. Reprinted with permission from [176]. Copyright 2013, Elsevier.

Figure 21. Schematics of the microstructures of bulk heterojunction layers and possible charge transport pathways: (a) binary P3HT:PCBM layer; (b) ternary P3HT:PCBM:FeS2 layer in regime I with a low loading of FeS2, where more densely packed P3HT and PCBM domains might be formed, resulting in an enhanced charge separation at P3HT:PCBM interfaces and possibly enhanced charge transport through these domains; (c) ternary P3HT:PCBM:FeS2 layer in regime II, where an increased FeS2 loading could adversely affect device performance likely by a combination of increased leakage current, charge recombination, and/or charge trapping in defect states; (d) ternary P3HT:PCBM:FeS2 layer in regime III, where a high FeS2 loading may completely diminish Voc and FF with large leakage current and possible shorting due to nanoparticle aggregation. (e) J–V curves for all ternary devices showing three distinct performance regimes. Reprinted with permission from [184]. Copyright 2013, Elsevier.

Figure 22. (a,b) Steady-state and (c,d) time-resolved PL quenching data from pristine QD (blue), binary polymer–QD (orange), and ternary polymer–fullerene–QD films (green). (a,c) refer to films based on 2.9-nm-sized QDs while (b,d) were on 4.3-nm-sized QDs. Pristine and ternary decays are fitted by double exponentials (red lines) dominated by the lifetimes displayed in the graph. The inset shows the polymer and binary QD film decays recorded at the peak of the hybrid PL. Reprinted with permission from [71]. Copyright 2013, Wiley.

254x116mm (96 x 96 DPI)

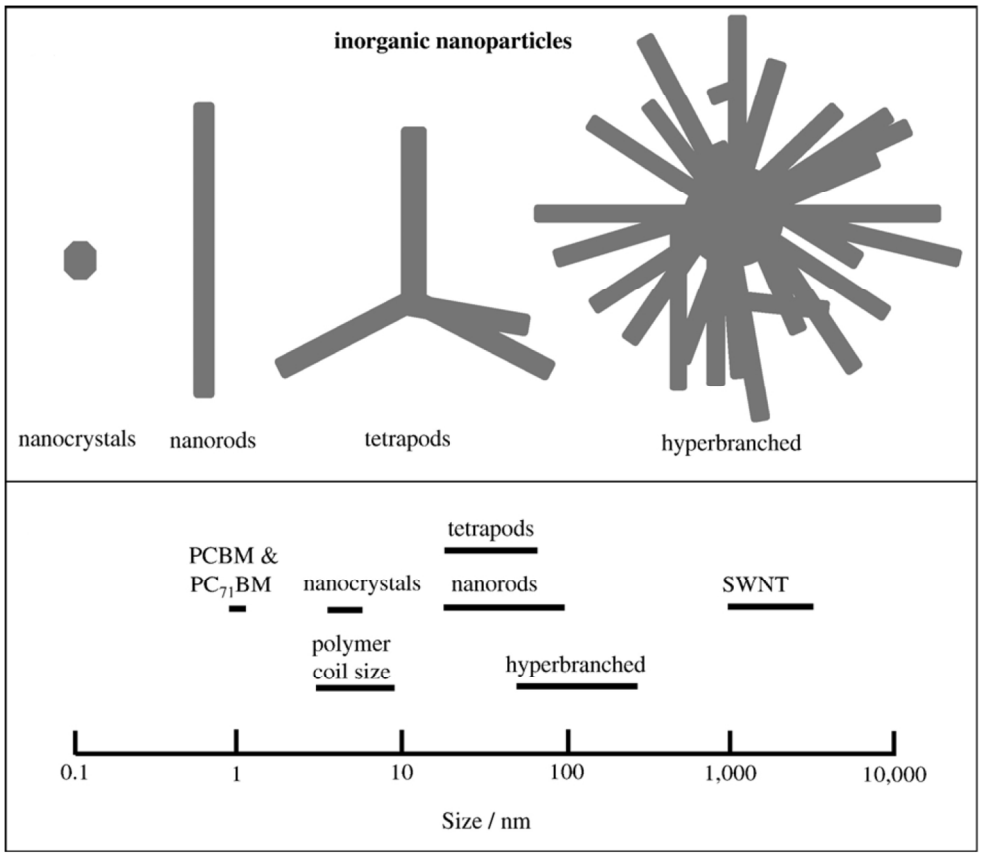

382x333mm (96 x 96 DPI)

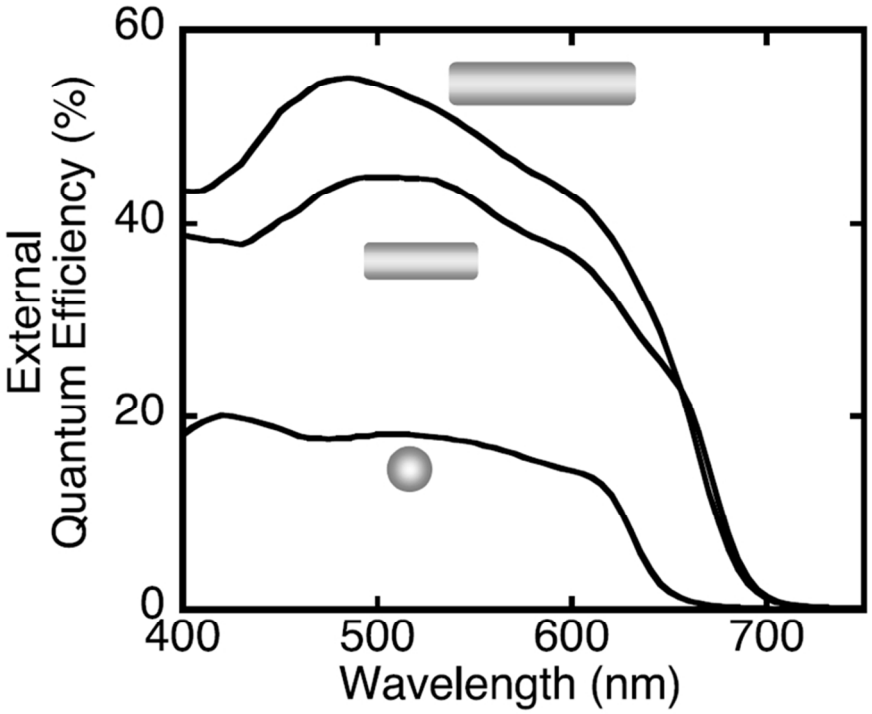

254x190mm (96 x 96 DPI)

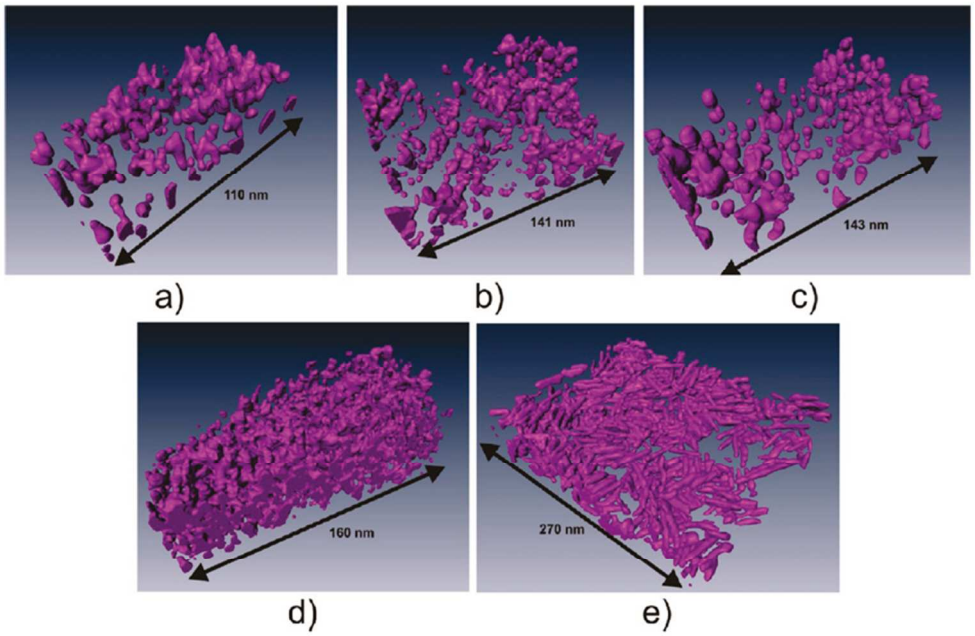

254x170mm (96 x 96 DPI)

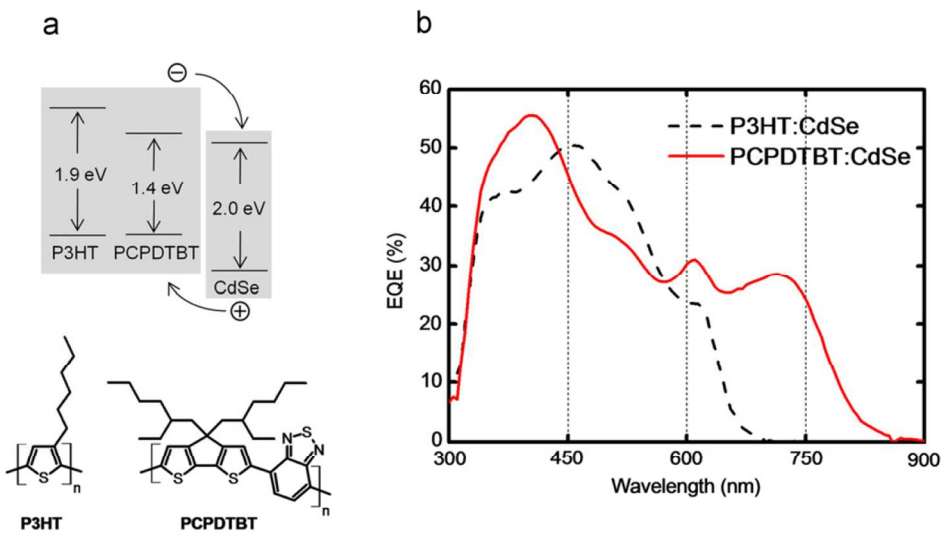

373x203mm (96 x 96 DPI)

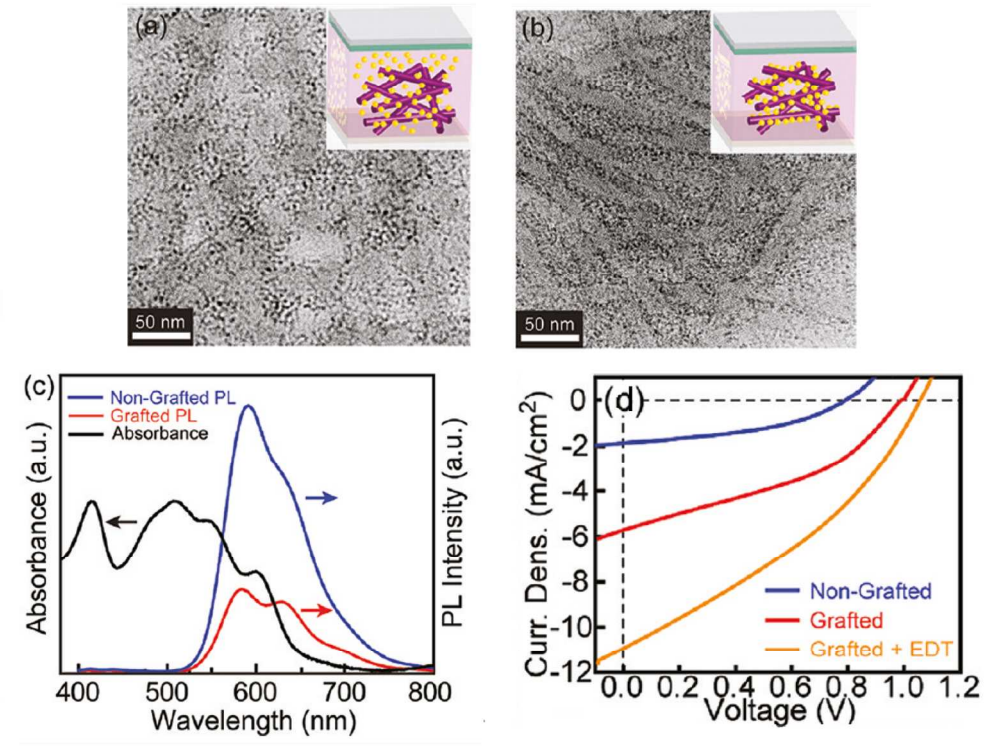

484x364mm (96 x 96 DPI)

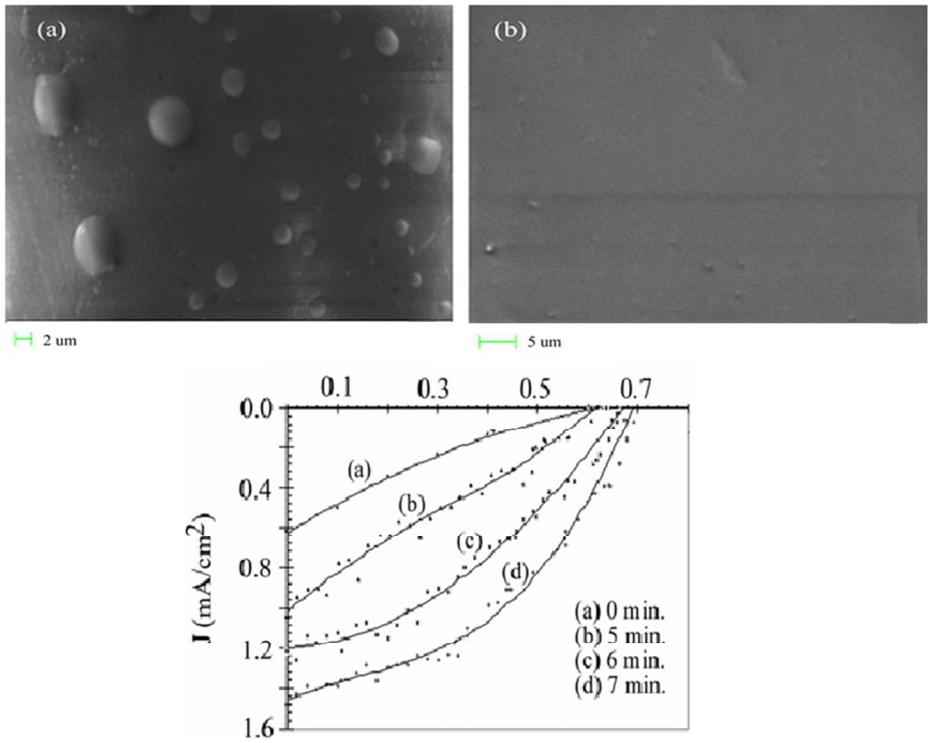

254x190mm (96 x 96 DPI)

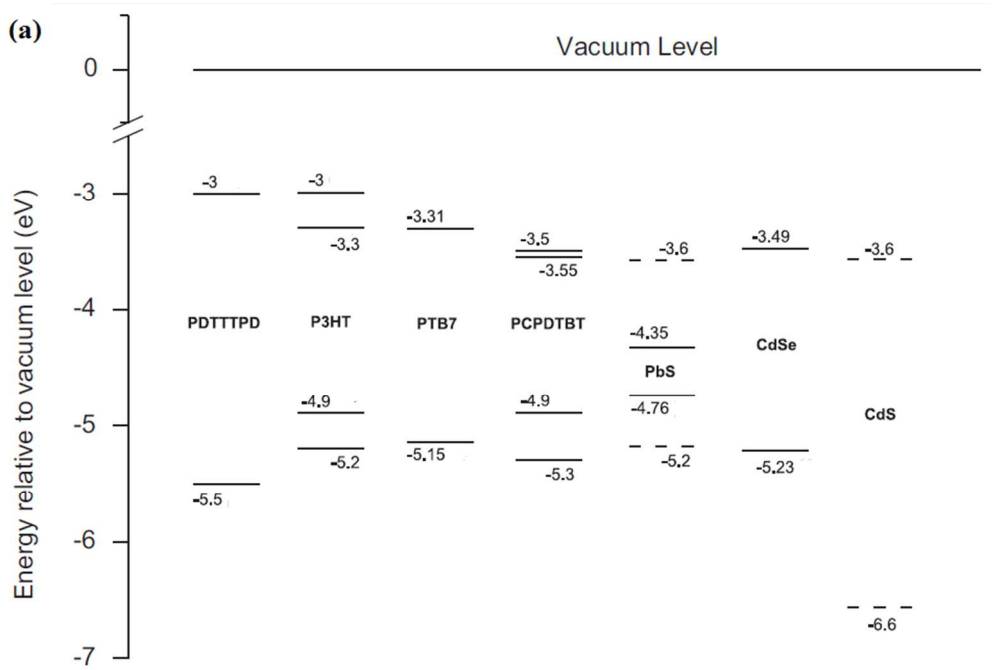

254x174mm (96 x 96 DPI)

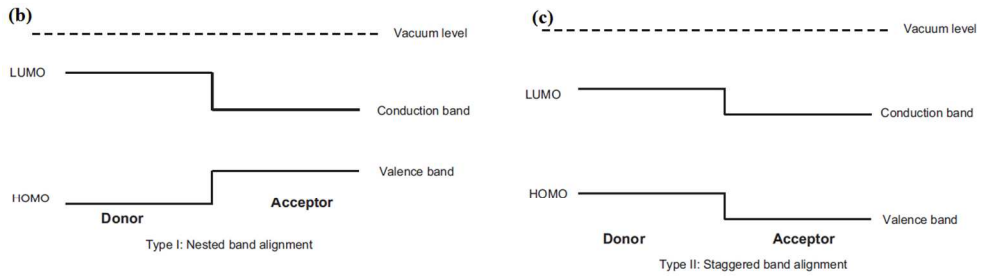

366x107mm (96 x 96 DPI)

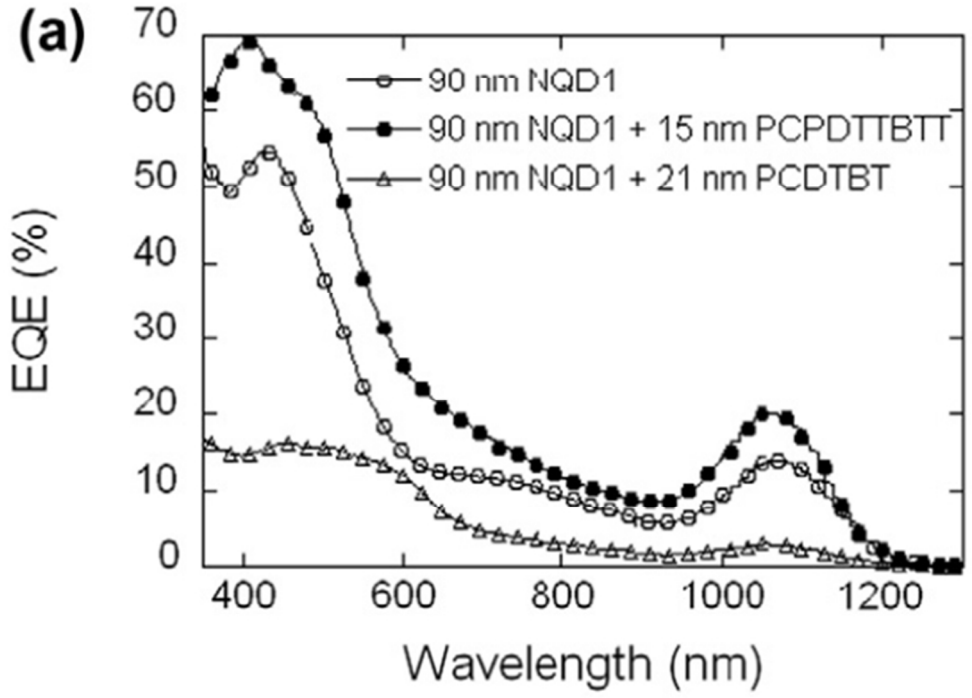

254x190mm (96 x 96 DPI)

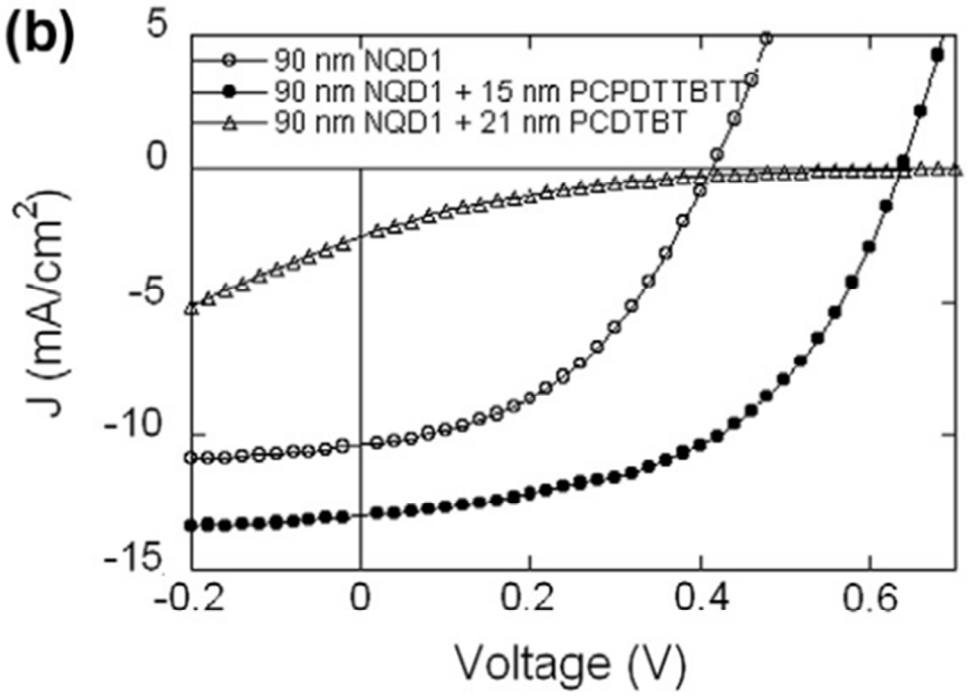

254x190mm (96 x 96 DPI)

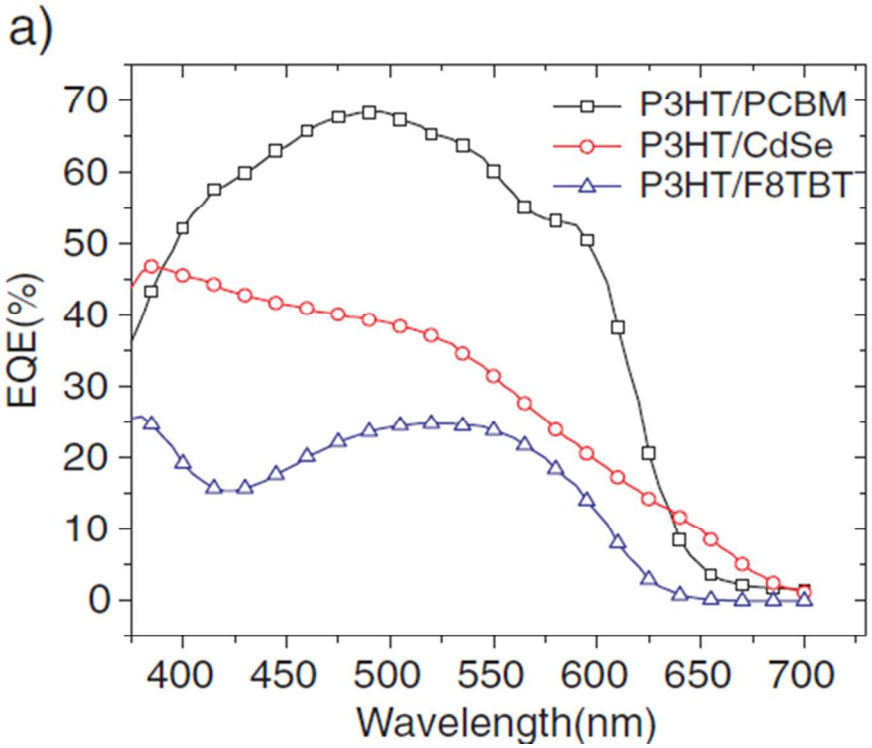

254x190mm (96 x 96 DPI)

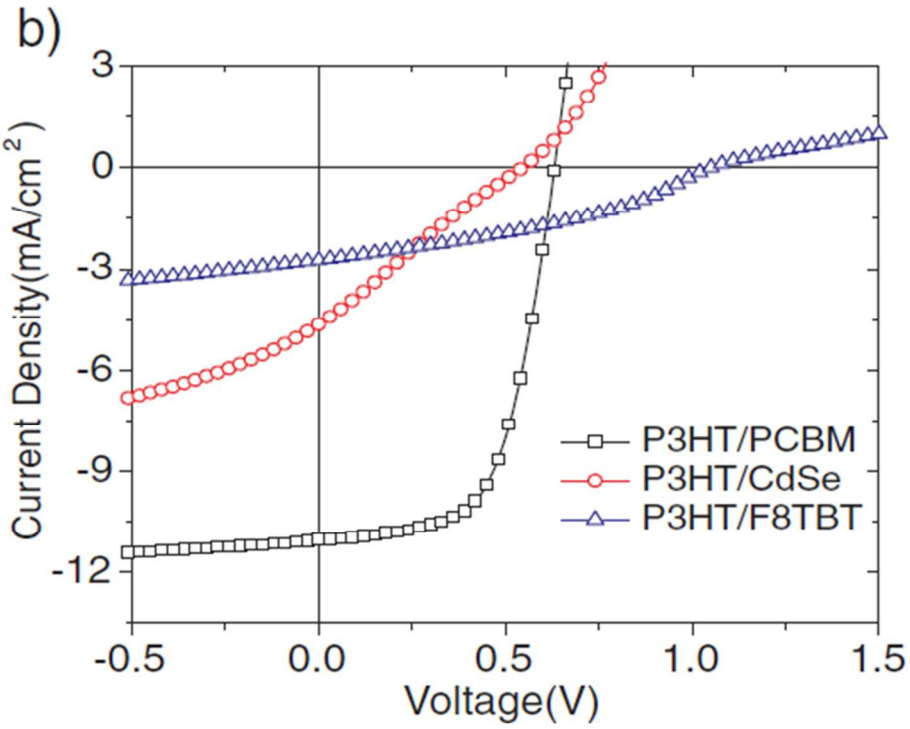

254x190mm (96 x 96 DPI)

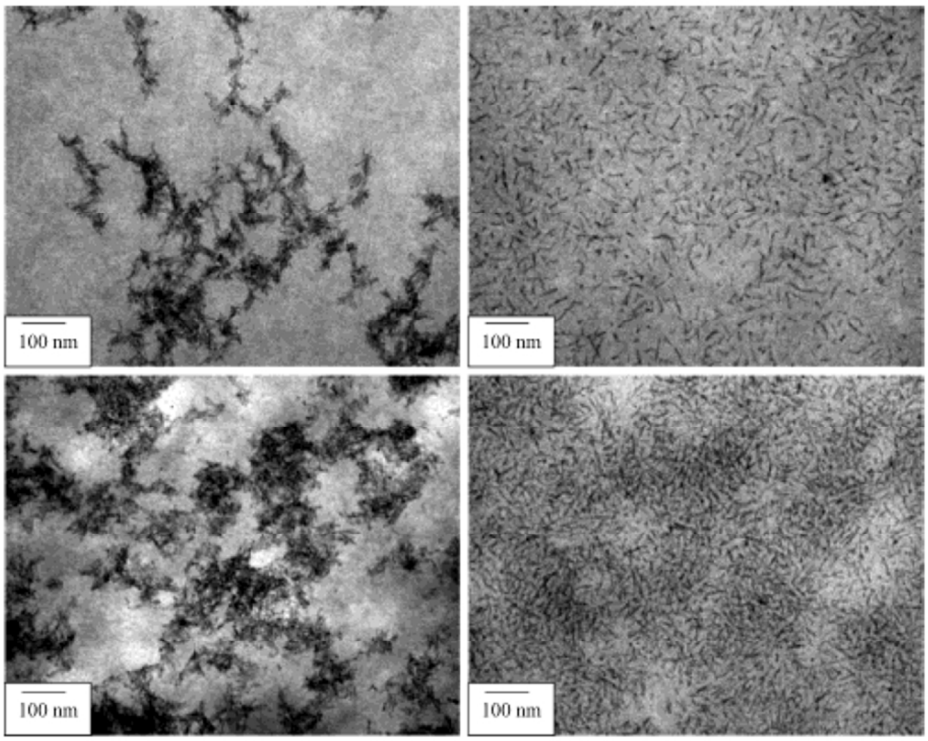

254x190mm (96 x 96 DPI)

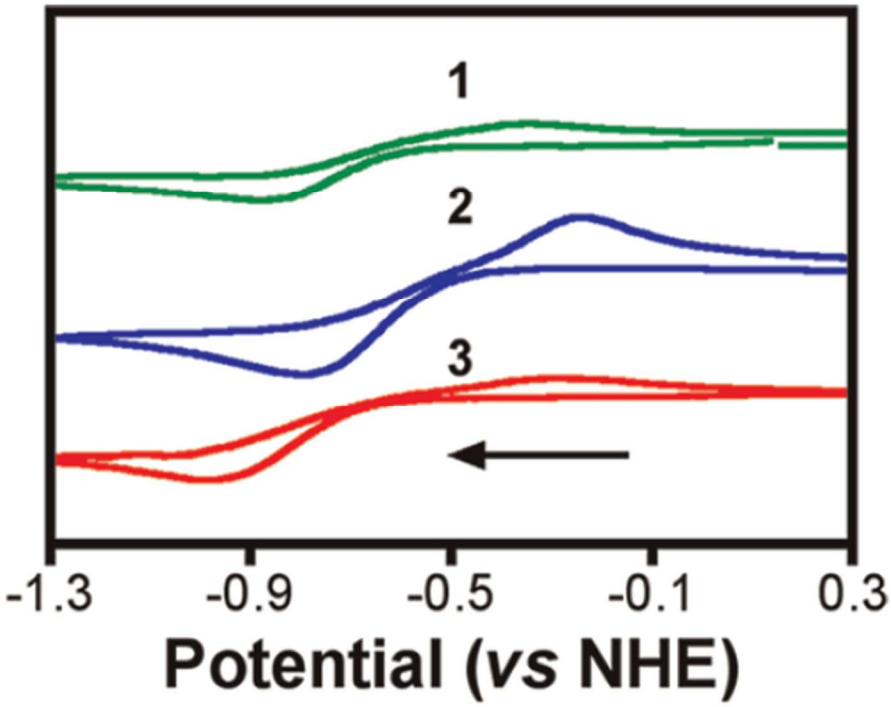

254x190mm (96 x 96 DPI)

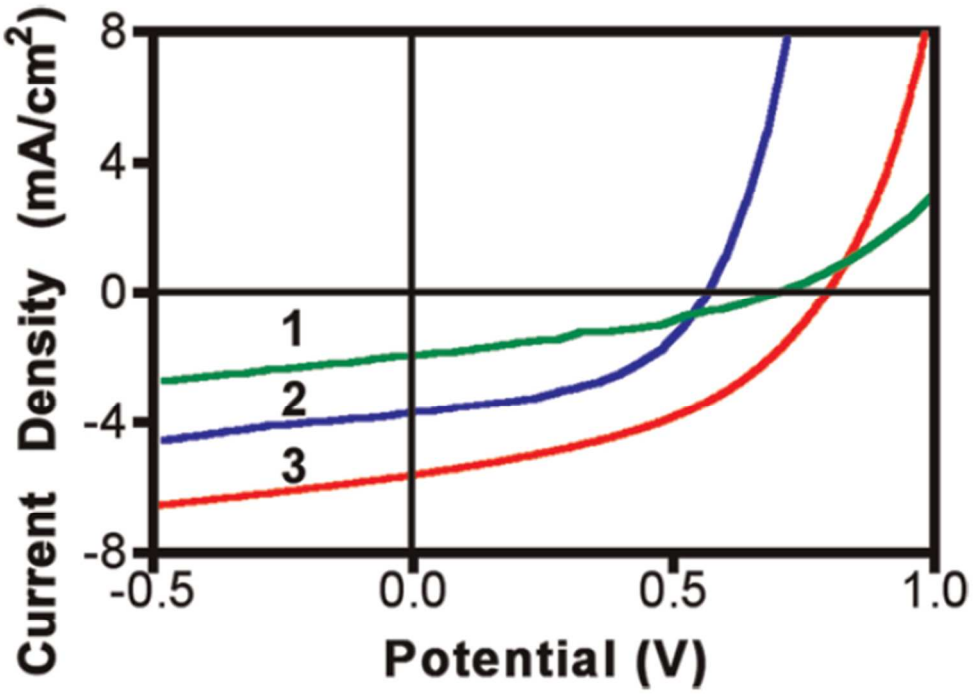

254x190mm (96 x 96 DPI)

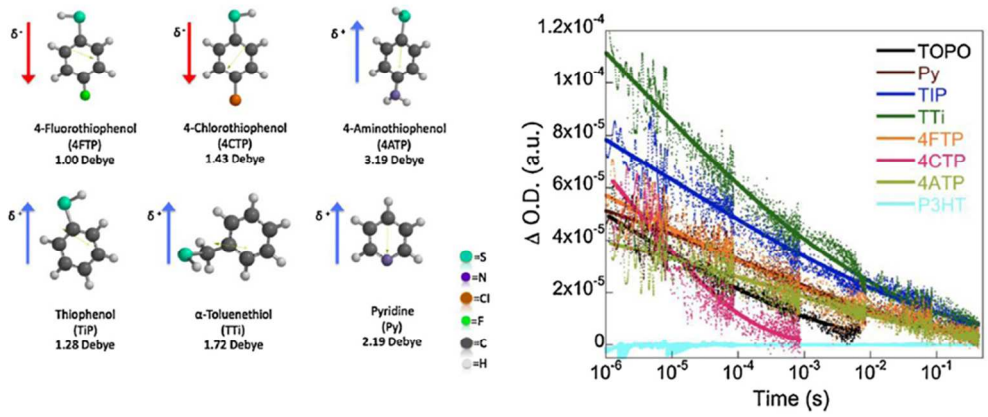

254x113mm (96 x 96 DPI)

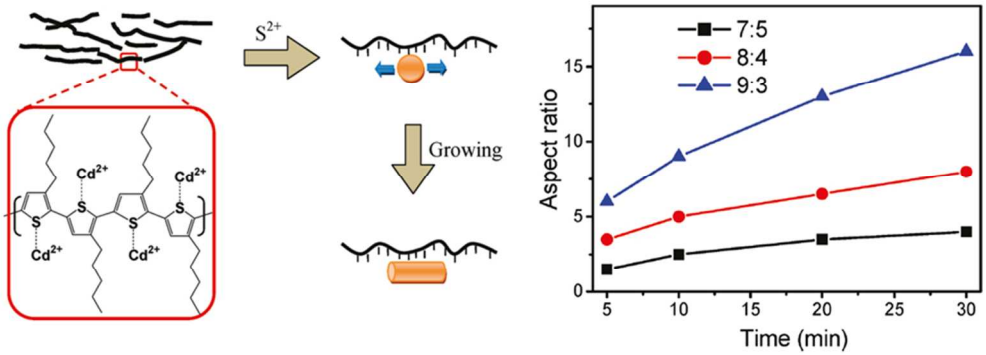

254x94mm (96 x 96 DPI)

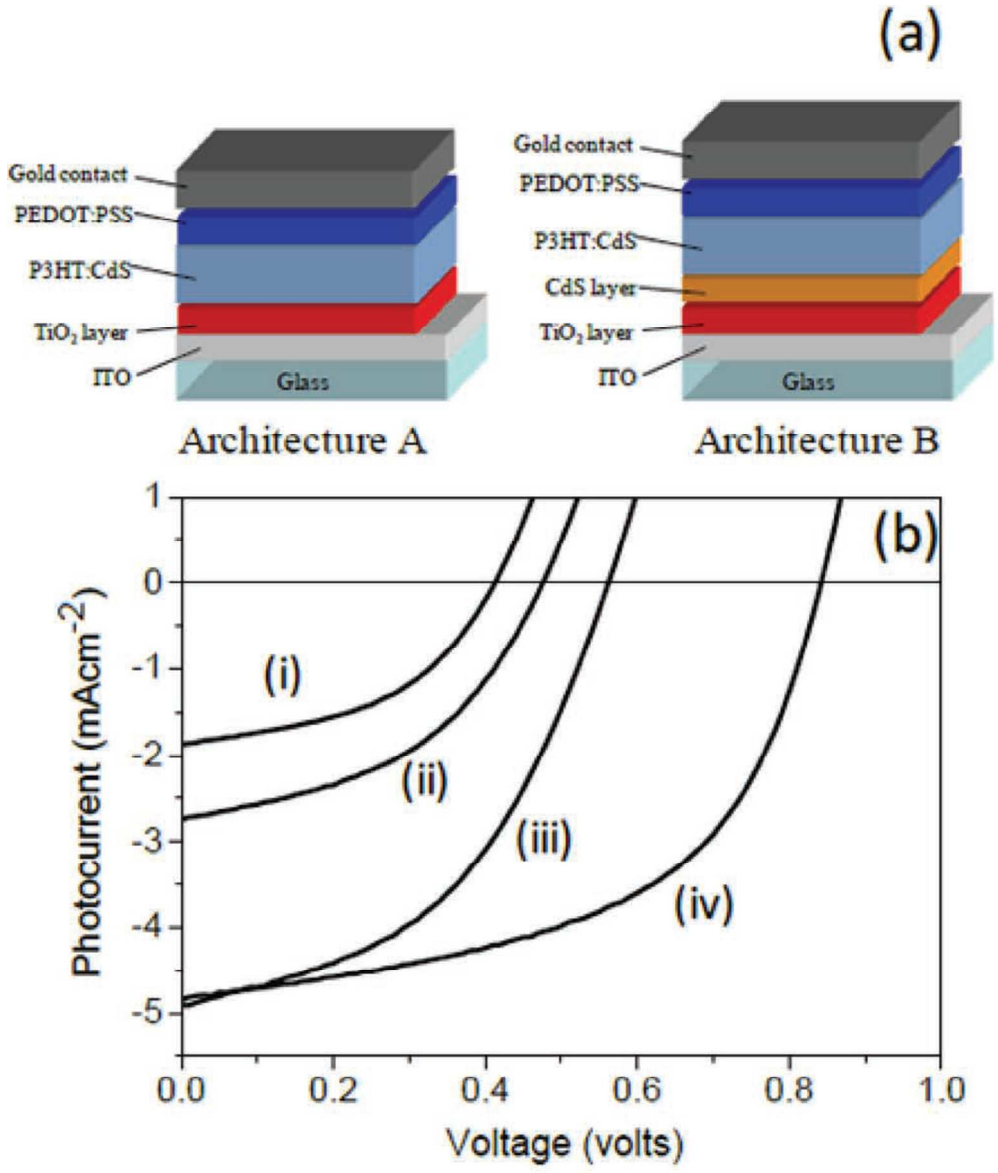

267x314mm (96 x 96 DPI)

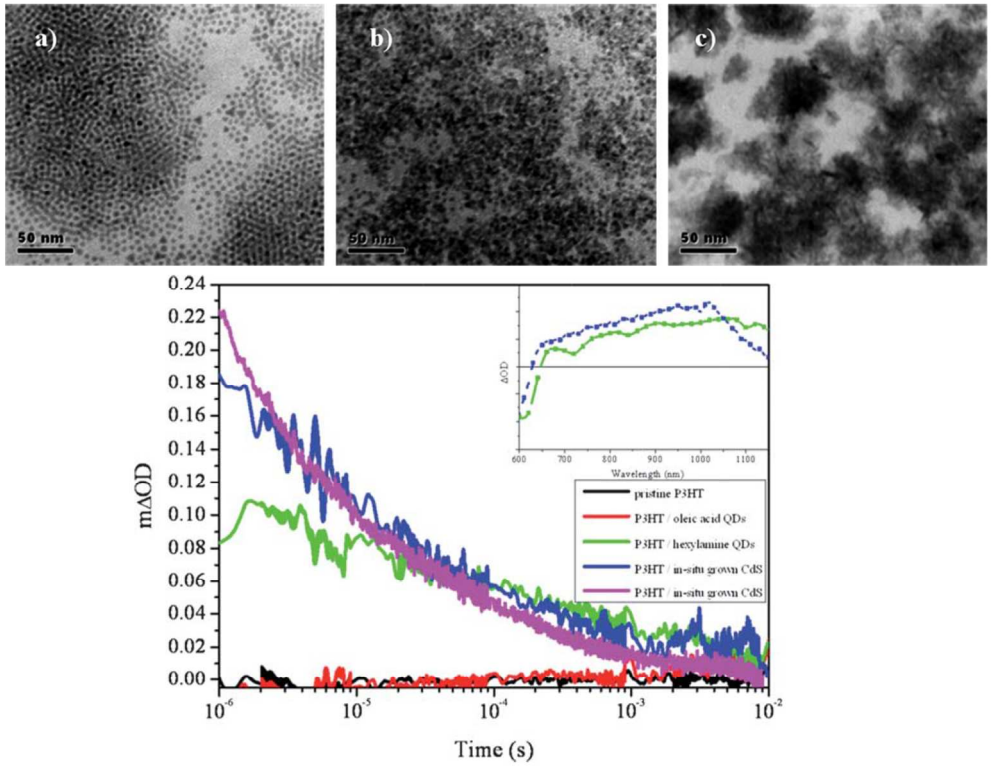

397x308mm (96 x 96 DPI)

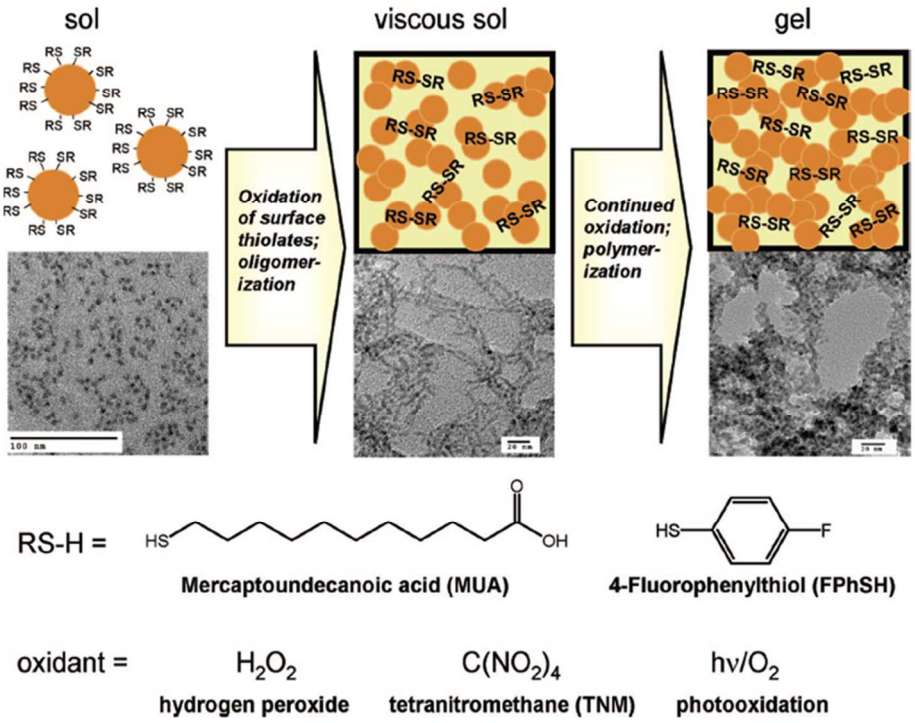

254x190mm (96 x 96 DPI)

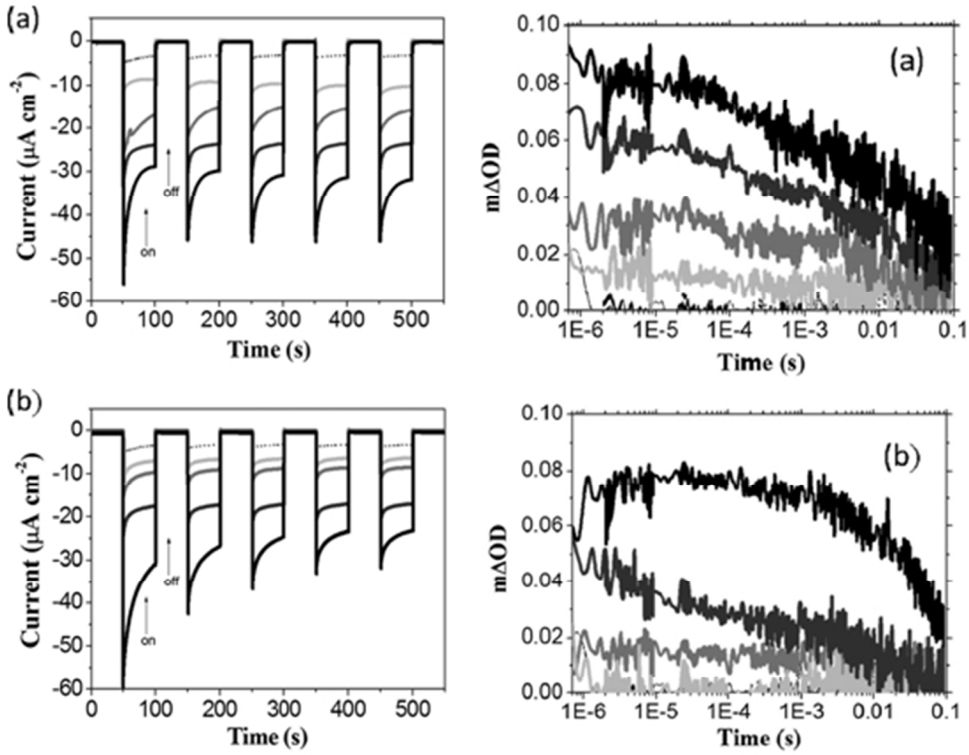

151x116mm (96 x 96 DPI)

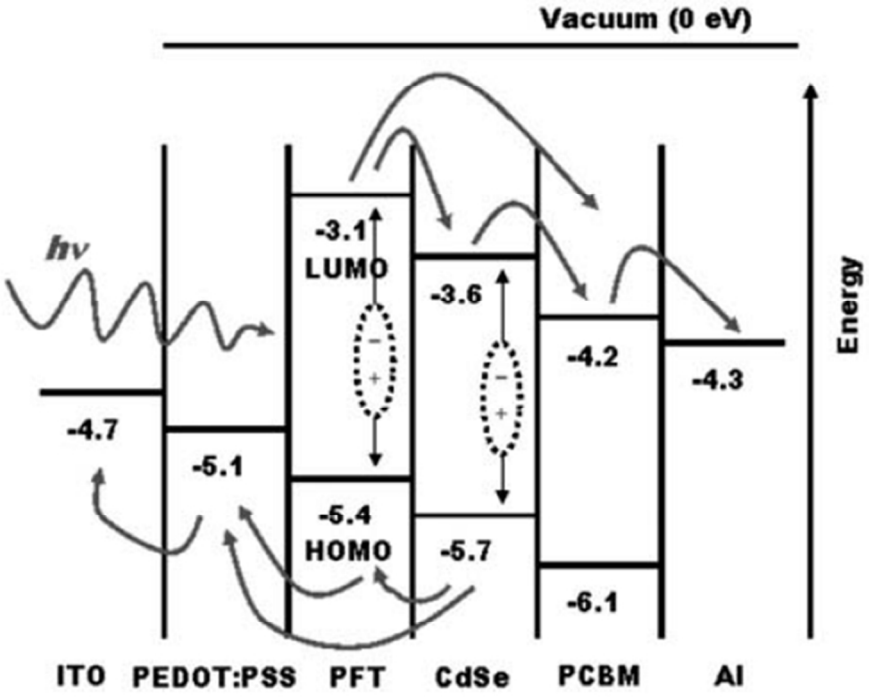

254x190mm (96 x 96 DPI)

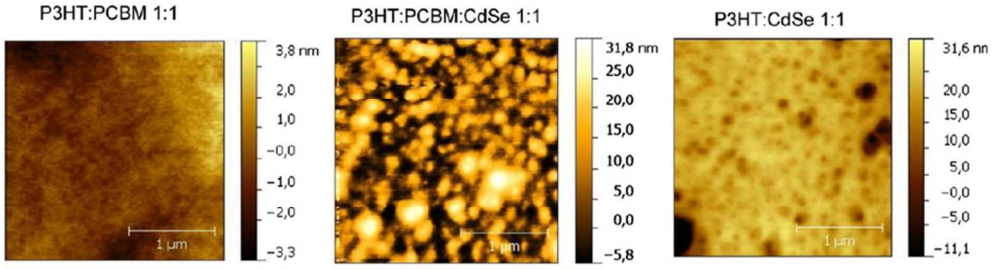

254x190mm (96 x 96 DPI)

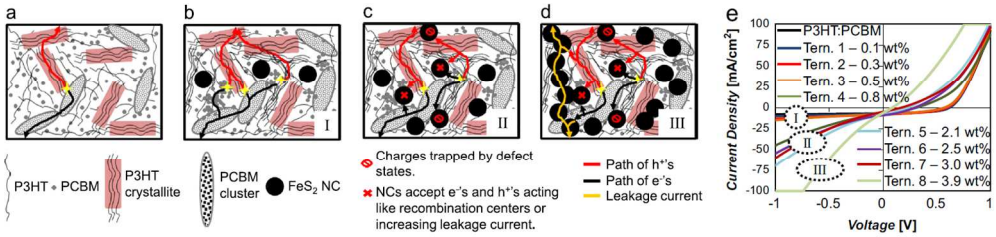

421x98mm (96 x 96 DPI)

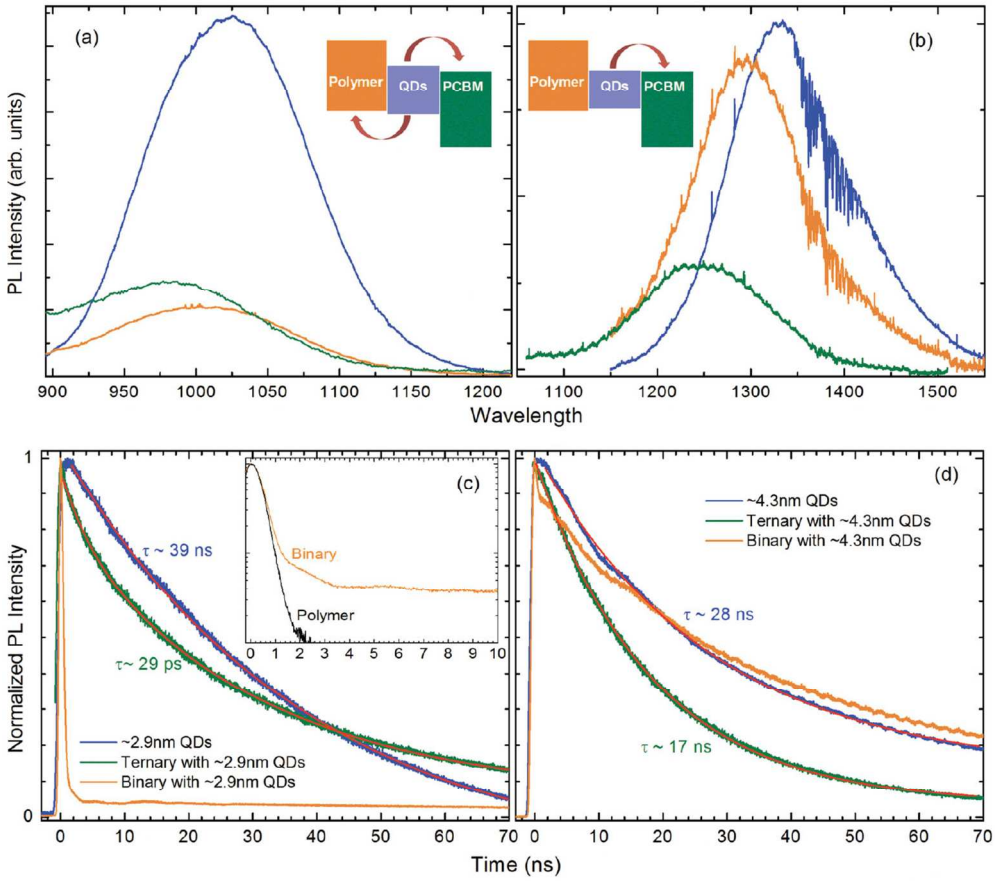

386x347mm (96 x 96 DPI)